Copper Additive Manufacturing – A Pilot Experiment

Soura Anabtawi
SEPT- MEME
McMaster University
Hamilton, CA
anabtaws@mcmaster.ca

Jan Boer
SEPT- MEME
McMaster University
Hamilton, CA
jan.boer@mcmaster.ca

Mo Elbestawi
(Supervisor)
SEPT
McMaster University
Hamilton, CA
elbestaw@mcmaster.ca

Marcin Magolon
SEPT- MEME
McMaster University
Hamilton, CA
magoloms@mcmaster.ca

***Abstract*—** Copper has been analyzed by multiple authors in recent months to investigate the appropriate Process-Structure-Property relationship that comes using the Additive Manufacturing process for use in the field of rapid prototyping and manufacturing optimization. In this paper, a brief overview of the research needs, and a completed study for the additive manufacturing specifications for optimized process-structure-properties is presented for the benefit of long-term growth of the additive manufacturing industry. This report will primarily cover the production processes in the selective laser melting field in a nitrogen based inert environment. Experimental observations will be drawn from the results primary analysis and the parameters for optimization will be presented. Finally, future possible solutions will be presented based on the findings as part of the discussion of this paper.

***Keywords*—** *Selective Laser Melting · Metal Additive Manufacturing · Copper Parts Fabrication*

I. Acronyms

AM	Additive Manufacturing
SLM	Selective Laser Melting
FDM	Fused Metal Deposition
EBM	Electron Beam Melting
LMD	Laser Metal Deposition
SEM	Scanning Electron Microscopy
EDS	Energy-dispersive X-Ray Spectroscopy
OFHC	Oxygen Free High Conductivity
LAM	Laser Additive Manufacturing
EDS	Energy Dispersive Spectroscopy

II. Notations

$\boldsymbol{P}$	Laser Power (W)
$\boldsymbol{v}$	Laser Scanning Speed (mm/s)
$\boldsymbol{h}$	Hatch Spacing (mm)
$\boldsymbol{t}$	Layer Thickness (mm)
$\boldsymbol{\gamma}$	Stripe Overlap (mm)
$\boldsymbol{\delta}$	Beam Offset (µm)
$\boldsymbol{E_v}$	Laser Energy Density (J/mm^3)
$\boldsymbol{c}$	Specific Gravity
$\boldsymbol{\rho}$	Density (kg/mm^3)
$\boldsymbol{T_m}$	Melting Temperature (K)
$\boldsymbol{T_a}$	Temperature Ambient (K)

III. Table of Contents

IV. TABLE OF FIGURES

V. Table of Equations

VI. Table of Tables

VII. Introduction

Additive manufacturing (AM) is a growing component of the manufacturing industry, capable of producing parts of fine and complex geometries otherwise unattainable through any other means of manufacturing. Theoretically, if a metal can be cast, then it should also be possible to apply it in the AM sphere. However, due to the difference between metal casting and metal AM, the relationship between the process and the resulting structure and properties of the manufactured part (PSPs) is inherently different between the two manufacturing technologies. Though research into the application of different materials in AM is ongoing, the number of known materials is still just a fraction of those that exist.

Through the development of the PSP, several properties must be evaluated to ensure optimal design parameters in the production of the new parts. These parameters include evaluation several common defects like porosity, cracking, oxidations and composites changes as a result of the printing process. On the other side of the coin, mechanical properties like hardness, wear resistance, tensile strength and fatigue requires evaluation as well as AM parts typically are produced in specialized situations where traditional machining is not possible, and a specific requirement is desired.

Throughout the project, this group will evaluate the viability of copper (Cu) using a Nitrogen (N) based inert environment in a selective laser melting (SLM) process, since in recent years, multiple researchers have published papers regarding the development of the PSP for copper-based AM materials with limited results for true production purposes, only covering some of the basics and identifying few items for review before a unique set of parameters could be produced for sustained use in AM.

VIII. Literature Review

A. Background on SLM

Common metallurgical defects can be observed in the process of SLM parts include porosity, cracking, oxidation and material composite changes. Each of these defects highlight unique mechanisms of their formation and has well studied causes. Each of these defects have a direct correlation on the desired mechanical properties that include hardness, tensile strength, wear resistance, and part fatigue. On the other side of the coin though, AM allows for the customization of materials which lead to ideal properties which can include designed hardness, tensile strength, wear resistance and fatigue.

1. Defects

a) Porosity

Porosity is the primary defect that can be experienced in any SLM process since porosity is defined as the insufficient or incomplete melting. Porosity is therefore the consequence of the trapped gasses in surface turbulence as well shrinkage in the part [1]. Porosity can easily be identified as they are mostly observed in the boundary layers, are irregularly shaped and greatly affected by the processing parameters including laser power, layer thickness, scanning rates and hatch spacing [2]. Highest fusion porosity can typically be observed in regions corresponding to incomplete melting across the interlayers while little porosity is observed when the laser is melting in a continuous process across layers [3]. Poor fusion porosity can thus be contributed to insufficient dissipation of the laser energy into the powder to a point where the previous layer cannot be re-melted to achieve complete bonding.

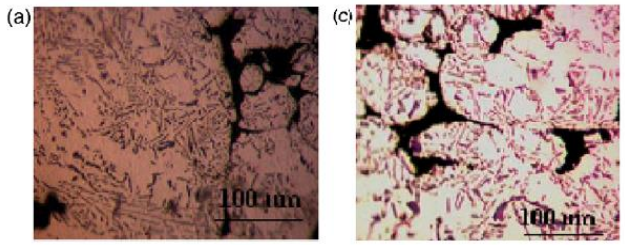

Figure 1: Optical micrographs of etched, polished parallel sections at 100J/mm^3 vs 67J/mm^3 porosity comparison [1]

As seen in Figure 1, a 33% reduction in power can easily cause large sections of porosity and start to show clear resemblance of powder particles used in the production. These elongated pores observed in Figure 1 is a result of a laser power of 200W, 120mm/s scan speed, 0.1mm hatch spacing and 0.25mm layer thickness; thus, through the use of Equation 1, a value of 64J/mm^3 can be obtained.

$$E = \frac{P}{vht}$$

Equation 1: Energy Density [4]

Another explanation given throughout literature is that low fusion porosity in the AM process is due to the buildup of gas in between the layers, causing an unstable scan track [5]. This unstable scan track is as a result of the forces active within the scanning track like the vapor cavity, fluid forces i.e. vaporization pressure liquid metal collapse [5]. Because it is believed that the vapor is either a result of the layer thickness entrapping gasses well below the surface or that it enters during the unstable time of the melt pool from the surround area [3], it is recommended by Fischer et. al. to have high amount of overlap of the fusion zone while keeping energy low to ensure the melted area is as small as possible while keeping layer thickness optimized for energy flow to reduce the overall temperature of the part once past the skin layers [6].

b) Cracking

Parts produced through the use of the SLM process are known to encounter cracking as experienced with aluminium alloy parts. The cracking is a result of the large expansion and contraction during melting and cooldown respectively, also observed in copper as a known issue with copper as through the welding of copper, cracks has been known to rapidly close during the process [7]. Provided that through the use of the SLM process, that is known to introduce additional internal stresses, when compared to the aluminium field where stresses are much higher than in copper, there is conjecture that through the minimization of dissipation energy through the substrate a reduction of the cracking can be realized [8]. Cao et. al. asserted that cracking during solidification is both a function of interaction between the strain rate, both internal and external, resulting from the shrinkage and ductility curve. Thus with the coefficient of volumetric expansion for aluminium being $69 \times 10^{-6} m/(m \cdot K)$, copper being $49.9 \times 10^{-6} m/(m \cdot K)$, and iron being $35.5 \times 10^{-6} m/(m \cdot K)$ [9], it can be concluded that due to copper sitting between iron and aluminium, more cracking that iron should be overserved though less than aluminium. This in turn means that there should be some observable cracking in copper prints due to it being a softer material than iron even though the elastic modulus is lower, as literature states that during the SLM process, the liquidus and solidus temperatures are depressed due to a lack of diffusion during the non-equilibrium rapid solidification [8]. Through the use of alloying elements, the narrowing of the critical solidification range can be achieved thereby allowing for the melt-pool to be altered which in turn will alter the way the cooling occurs and thereby the cracking observed. Finally, the solidification cracking susceptibility of the SLM process can also be expected to be process sensitive as there is reports that state the existence of the optimum laser energy density at which parts are fully dense and obtainable. Anything above the

value the optimal value, cracking will occur as there is high thermal stresses, long liquid lifetime and low liquid viscosity and anything below the optimal value, balling would occur due to the instability of the liquid through the Margoni convection [1].

c) Oxidation

Oxidation films has been known to inhibit the SLM process as it promotes the balling effect and prevents the wetting across previous sintered or melted layers. This effect also may end up with oxygen in the melt pool, thus changing the alloying composition, through either alloying on the particle or gas entrapment during the turbulent flow of the SLM process [10]. As the SLM process does not have uniform scan tracks, i.e. track position varies with time, rapidly fluctuation tracks tend to entrap the shielding gas or air, thereby resulting in the oxidation or pocket defects of the part as can be seen in Figure 3. There are several papers that indicate the reactivity of copper with oxygen in the casting process as seen in Campbell's [11] book. As Campbell explains, there is a thin layer of oxidation on the surface of the liquid that will hold the surface stationary and affect the viscosity and can only be removed if violently stirred. Campbell also notes that as the oxide layers convert to crystalline structures on cooldown and they thicken, multiple phases and structures can be observed. Finally, Campbell indicates that there are only films experienced with copper when the temperature is above the solubility limit as seen in Figure 2. Louvis et. al. [12] points out that these oxide films are known to cause issues in the SLM process as the process is required to break through the film in order to achieve fully dense parts, thereby requiring higher laser power.

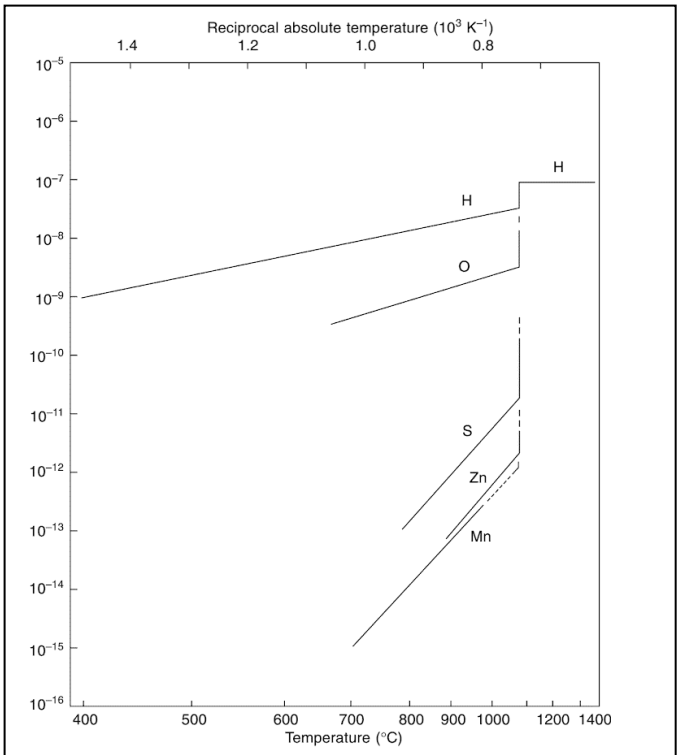

Figure 2: Diffusion coefficients for elements in copper [11]

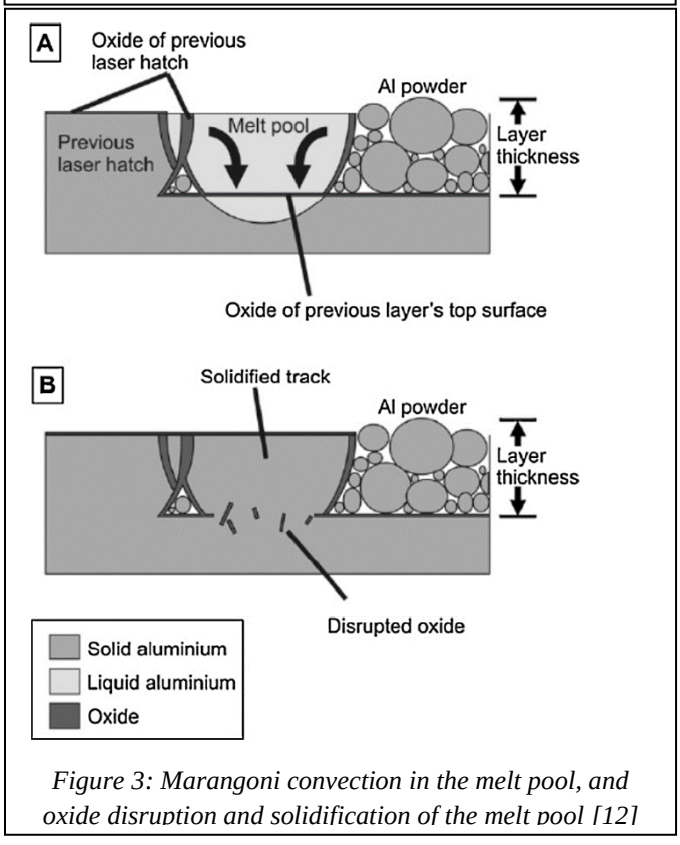

Figure 3: Marangoni convection in the melt pool, and oxide disruption and solidification of the melt pool [12]

d) Composite Changes

As copper is a highly reactive metal when in nanoparticle form, several researchers have

attempted to protect the refined metal from its environment to prevent oxidation. Many produces or fine metal powders would coat their powders in organic layers or polymers [13], thereby preventing oxidation when handled in an open-air environment. This coating, however, causes issues with electrical and thermal conductivity of the material and has therefore been studied to see if there is the possibility of coating the material with ultrathin layers to ensure optimal performance of the material. Chen et. al. [14] used graphene as a coating material, as graphene is both electrically and thermally conductive as well as only absorbs 2.3% of the visible light spectrum per layer. It should be noted however that during the SLM process, intrinsic vaporization of elements can occur as the melt-pool forms at the liquid vapor interfaces. This vaporization would thus remove the protective layer of the graphene as graphene combusts at 350°C [15] to form CO_2 or CO. Also, as carbon is a strengthening element in metals, ideal properties might be obtained by the inclusion of carbon nanoparticles in the material through the AM process. Thereby controlling the laser beam power and density distribution, as well as the particle inclusions, a specific alloy can be achieved by vaporization of elements from the base powder. Alternatively, through the use of high scanning speeds with medium or high power, the loss of alloying elements can be avoided [16].

2. Mechanical Properties

e) Hardness and Wear Resistance

An advantage of the SLM process is that hardness can meet and sometimes exceed the hardness that can be achieved by alternative processes like casting. Buchbinder et. al. [17] found that as the scanning speed increased, so did the parts hardness. Buchbinder et. al. also showed that this increase was not affected by the hatch spacing. Mercelis et. al. [18] found that the induced residual stresses were an advantage of the SLM process as it provided a reasonable enhancement in the parts hardness at sufficiently high densification. According to Gu et. al. [19] low scanning speed attributed to low densification rate due to the formation of thermal microcracks and the formation of coarser grains. As Gu et. al. further explains, that the densification of the structure and the microstructure properties of SLM produced parts shows that the increase in hardness show a correlating increase in the wear performance as well. Between these three studies, it can be reasonably be concluded that there should be an ideal hardness that can be obtained by varying the scanning speed while also reaching high densification of parts as well as keeping good wear resistance on the parts.

f) Tensile Strenght

Tensile strength, primarily dependent on the fractional density of the part, has been shown to be a trend between the scanning speed and laser power as seen in Figure 4.

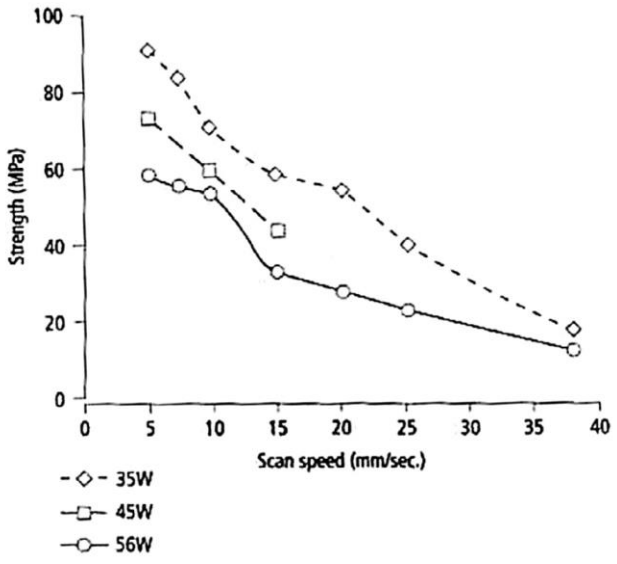

Figure 4: Tensile strength for SLS processed bronze-nickel parts [20]

Also included in the variance of the fractional density is the powder characteristics as SLM studies has shown that higher density can be obtained by using a lower layer thickness [20]. Kruth et. al. [21] also demonstrated that short scanning vectors cause more localized energy on the part than those of long scanning vectors, since

the short vectors does not allow for full temperature decay, thereby decreasing the tensile strength. Consequently, Chlebus et. al. [22] showed that scanning vectors varying and averaging out at 45° will provide the median of the short and long vector tensile strengths. Furthermore, Chlebus et. al. found that the direction of the parts build, i.e. if it was slanted on the plane, would similarly influence the residual stresses and elasticity. Finally, Spierings et. al. [23] found that depending on the powder granulations size, the resulting tensile strength showed that finer powders produced better results for the tensile strength. Concluding therefore, that through the use of an alternating scanning strategy, finer powders and scanning speeds, an optimal design for tensile strength can also be reached though not necessarily alongside the production of the hardness.

g) Fatigue

Similar to the fatigue behavior of conventional sintered parts, the presence or absence of microstructural defects including porosity and oxidation can cause a fatigue line. These lines are typically found in between the layers of the part and is seen as an occurrence of low melting temperature. These lines in turn causes stress concentration resulting in the reduction of static and dynamic strengths of the parts. Wang et. al. [24] investigated the crack path, propagation and point of initiation through the use of surface replication in the four-point bending fatigue tests. Wang et. al. discovered that the fatigue behavior was controlled by the layer structures as well as the pores on or underneath the surface. Wang et. al. concluded that the most beneficial effect of high density was the reduction of pores where microcracks typically initiated. This showed to be especially true when porosity was high in that microcracks would readily form and propagate through the material, as can be seen in Figure 5.

Thus, through the solidification of the parts, it can be concluded that there are lower chances of fatigue stresses causing park breakage and should therefore be one of the primary goals of any AM part.

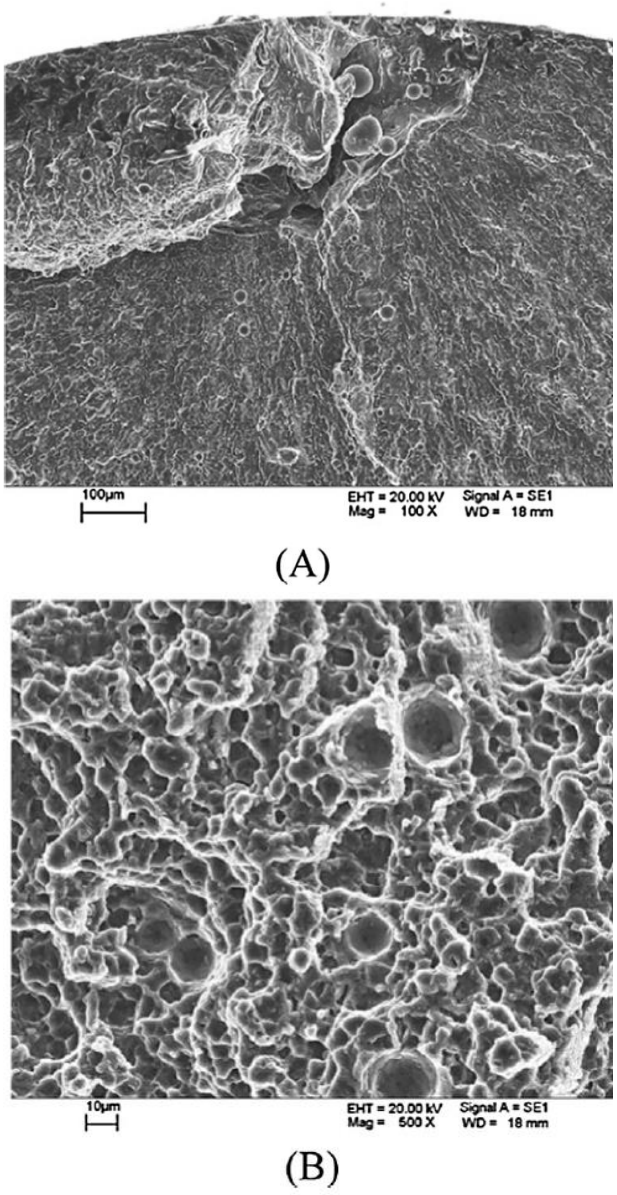

Figure 5: (A) – Crack initiation site due to porosity (B) – Area of fracture [55]

B. Copper as a Material (99.7% Pure)

3. Benefits with Copper

Copper additive manufacturing is rapidly expanding and has recently gotten the attention within the AM industry. According to SmarTech Analysis, a leading provider of AM market data and analysis, it is predicted that the additive manufacturing with Copper will grow 51% through 2027 [25]. This forecast is based on a market study that tracked the copper powder shipments to AM users. Copper alloys exhibit outstanding

mechanical properties and are low in cost [26] which makes them a preferred choice for tool inserts. Figure 6 shows the various end user market for copper powder in the year 2018. This shows about 45% growth from previous year.

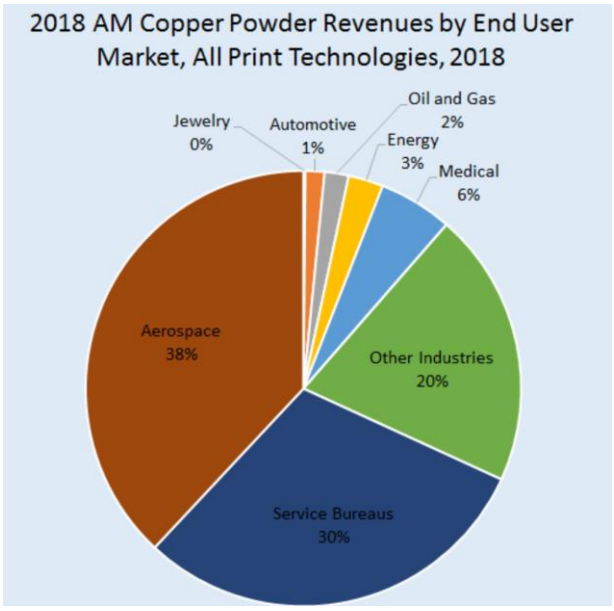

Figure 6: End market user for Copper powder [25]

The two main properties of Copper that make it indispensable are its electrical and thermal conductivity [3], but there are many properties that contribute to the uniqueness of Copper. They are as follows:

- **Electrical Conductivity**: Copper has the highest conductivity of any non-precious metal and one that's 65% higher than aluminium. When this is combined with its high ductility, medium strength, ease of joining and good resistance to corrosion, it makes copper the first choice as a conductor for electrical applications. such as cables, transformer and motor windings, and busbars.
- **Thermal Conductivity:** Copper is an exceptional conductor of heat (about 30 times better than stainless steel and 1.5 times better than aluminium). This leads to applications where rapid heat transfer is required such as heat exchangers in air conditioning units, vehicle radiators, heat sinks in computers, heat sealing machines and televisions, and as water-cooled furnace components.
- **Corrosion Resistance:** Copper is low in the reactivity series. This means that it doesn't tend to corrode. This is important for its use for pipes, electrical cables, saucepans and radiators. It also means that it is well suited to decorative use. Jewellery, statues and parts of buildings can be made from copper, brass or bronze and remain attractive for thousands of years.
- **Alloys Easily:** Copper can be combined easily with other metals to make alloys. The first alloy produced was copper melted with tin to form bronze –Much later came brass (copper and zinc), and – in the modern age – copper and nickel. The alloys are harder, stronger and tougher than pure copper.
- **Easily Joined:** Copper can be readily joined by brazing, soldering, bolting or adhesives. In industry, this is very useful for plumbing pipework and joining busbars, which are vital elements of power distribution systems.
- **Ductile:** Copper is a ductile metal. This means that it can easily be shaped into pipes and drawn into wires. Copper pipes are lightweight because they can have thin walls. They don't corrode, and they can be bent to fit around corners. The pipes can be joined by soldering and they are safe in fires because they don't burn or support combustion.
- **Tough:** Copper and copper alloys are tough. This means that they were well suited to being used for tools and weapons. Imagine the joy of ancient man when he discovered that his carefully formed arrowheads no longer shattered on impact. The property of toughness is vital for copper and copper alloys in the modern world. They do not shatter when they are dropped or become brittle when cooled below 0°C.

- **Non-magnetic:** Copper is non-magnetic and non-sparking. Because of this, it is used in special tools and military applications.

Copper is widely used in various industries such as aerospace, automotive and electronics and can be used in applications such as heat exchangers, water cooled molds and electronic components [25]. The thermal conductivity of pure copper and its alloys makes it the best candidate for thermal and electrical management applications [27]. Table 1 shows common thermal properties of copper.

Material Properties						
Specific Heat (J/kg*K)	Density (kg/m^3)	Temperatures (ºC)		Thermal (at ED > 50)		Emissivity
		Melting	Boiling	Conductivity (W/m*K)	Diffusivity (mm2/s)	
376.812	8940.00	1085.00	2562.00	395.00	117.26	0.05

Table 1: Common Thermal and Physical Properties of Copper

4. Challenges with Copper

The very same properties that makes copper so great makes it extremely challenging to process in additive manufacturing. As can be seen Table 2, the properties of the typical alloys that have been processed in AM are very different to Copper's properties in Table 1. Since none of the previously produced materials have similar properties in terms of conductivity and diffusivity, a challenge is encountered. The main difficulties with additively manufacturing Copper are as follows:

- **The high conductivity of Copper** presents complications during processing since it will rapidly conduct the heat away from the melt area and therefore result in high local thermal gradients [28]. Furthermore, the high conductivity can lead to layer curling, delamination and ultimately lead to build/part failure.
- **The high reflectivity of Copper** is another main property that creates a problem during the deposition process in additive manufacturing. The high reflectivity generally means low absorptivity of the laser power. This means that only a small portion of the laser energy is actually absorbed by the powder bed. Which means that a large amount of energy is needed in order to ensure full melting during the SLM process [26]. The low absorptivity causes solidification cracking and can lead to porosity.
- **The high diffusivity of Copper** is a measure of the rate of heat transfer of a material from a hot side to a cold one. It is related to the thermal conductivity.
- **Oxidation** is a concern when dealing with powder Copper. Copper is generally very reactive with oxygen, however, when in powder form it tends to be sensitive to oxidation. This makes the handling and storage of copper powder to be critical as to avoid the powder

Reference Material	**Specific Heat (J/kg*K)**	**Density (kg/m^3)**	**Conductivity (W/m*K)**	**Diffusivity (mm2/s)**
SS 361L	468.00	8000.00	16.30	4.35
Inconel 617	419.00	8360.00	37.10	10.59
Titanium	544.28	4500.00	25.00	10.21

Table 2: Properties of common AM materials.

from oxidizing. Surface oxides pose a complicated issue as they will result in porosity in the deposits. During the laser processing, the oxides decompose into copper and oxygen has which leads to rapid expansion that contributes to the porosity formation in the deposit [28]. Furthermore, the melting process becomes complicated due to the oxides process. This is because the melting point of Cu is 1083˚C whereas the melting point of CuO and Cu_2O is 1336˚C and 1230˚C respectively [26].

- **Copper particle agglomeration** is another problem that is encountered when dealing with copper powder. The copper powder particles tend to accumulate and form clusters which reduces the overall flowability of the powder and impedes powder deposition [28].
- **Balling Effect** due to surface tension in the molten state [26] can cause the formation of discontinuous scan tracks and poor inter-line bonding properties [29].
- **High Ductility** hinders post build powder removal and recovery.

5. Copper Effects in AM

Pure copper has been known to have a relatively high thermal conductivity which facilitates rapid cooling. With coppers thermal conductivity sitting at 385W/m·K [30], almost 1.9x that of aluminium and 4x that of steel, thermal conductivity in the AM production poses significant challenges in the production of pure coppers.

This high conductivity is the biggest issue some papers study as high thermal gradients result from the rapid melt pool cooling, which in turn results in layer curling, layer delamination or even total part failure. Additionally, copper is highly susceptible to oxidation with a standard reduction potential of 0.16 compared to iron at 0.04 [31]. Frigola et. al. [32] successfully produced AM parts using the Electron Beam Manufacturing (EBM) process in conjunction with Oxygen Free, High Conductivity (OFHC) copper. They also note that in their process, grains of Cu_2O were present and extra grains were included in the boundaries as the process pulled in any residual oxygen and water in the surrounding area during production. This in turn brought the density down on the parts as well as decreased the electrical conductivity by 5%. As can be seen in Figure 7, the oxides formed not only disrupt the grains but also the included boundaries and the resultant microstructure, creating porous materials.

As many defects are associated with the density and the proper forming of grains, oxide inclusion should therefore be the top priority for reduction. Though Frigola et. al. successfully produced the AM parts using the EBM process using the OFHC powder, SLM processes have not yet caught up due to the high reflectivity and thermal conductivity of the OFHC powder.

With the properties of the OFHC, other test runs have shown high amounts of cracking and porosity using the SLM process.

El-Wardany et. al. [28] showed that for the SLM process, high power and low speeds are required to successfully complete while keeping the designed physical and mechanical properties within margins of error. El-Wardany et. al. however noted that for the SLM process, their samples required the treatment of powders for the purpose of reducing the included oxides and the generation of the oxides after powder production.

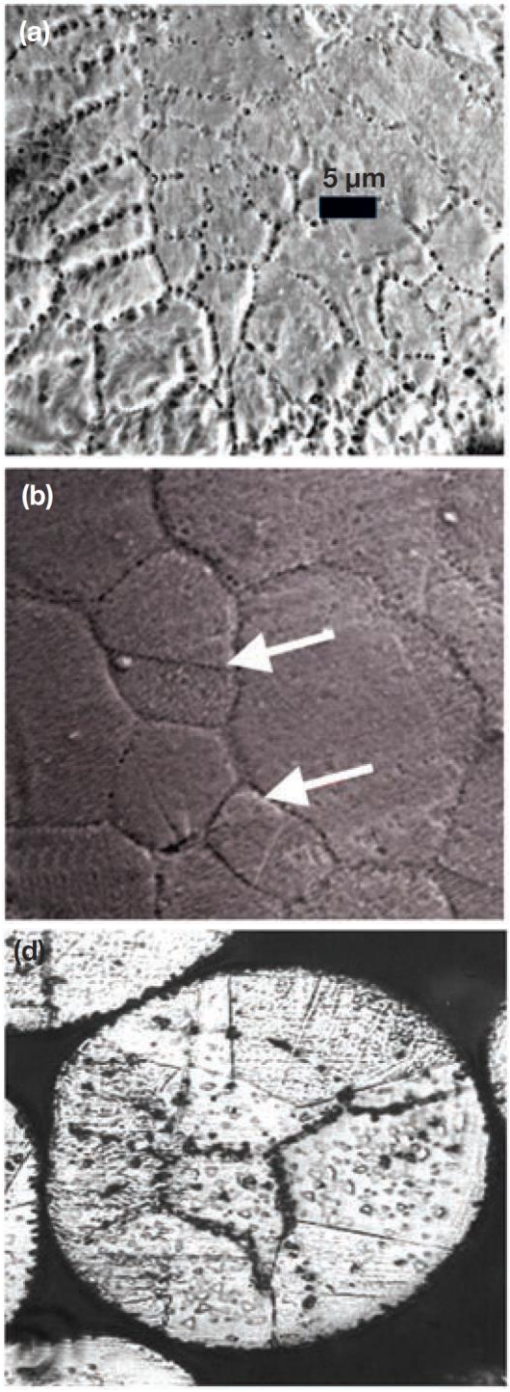

Figure 7: (A) – High concentration of oxygen in grain boundaries
(B) – Oxides affecting grains and boundaries
(C) – Equiaxed grain structure with oxide inclusions [32]

a) Material Conductivity

The prime factor in the widespread application of pure copper, the high electrical conductivity is second only to that of silver and first among all non-precious metals. As a result, copper was set as the industrial standard to which electrical conductivity is compared, the electrical conductance of annealed copper is $5.8 \times 10^7 \, S/m$ or 100 percent IACS, in contrast, common materials such as aluminium and stainless steel have an electrical conductance of $3.5 \times 10^7 \, S/m$ and $1.45 \times 10^7 \, S/m$ respectively, resulting in a loss of approximately 40 and 75 percent [33].

In order to increase the tensile strength of copper it is common to apply various alloying elements such as Tin, Zinc, Nickel, and Lead as seen in Figure 8.

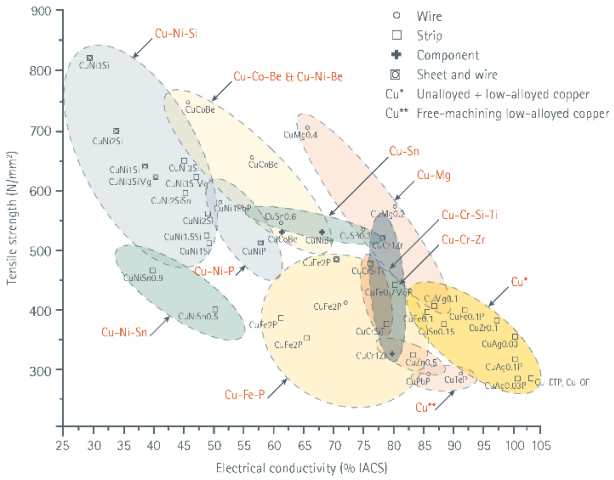

Figure 8: Tensile Strength vs Electrical Conductivity for different copper alloys [44]

However, the alloying of copper can affect the electrical conductivity. Figure 9 shows the incredible sensitivity of copper to the presence of impurities and alloying elements. CuSn0.15, a common copper alloy used extensively the automotive and aerospace industry, has an electrical conductivity of 88% IACS at 0.15% Sn, however, at 0.2% and 0.5% Sn the electrical conductivity falls to 83% and 70% IACS respectively. Impurities of even 0.1% Si can result in a loss of approximately 30% IACS [34]. Therefore, the desired electrical conductivity must first be established in order to guarantee that the manufactured part meets design specifications.

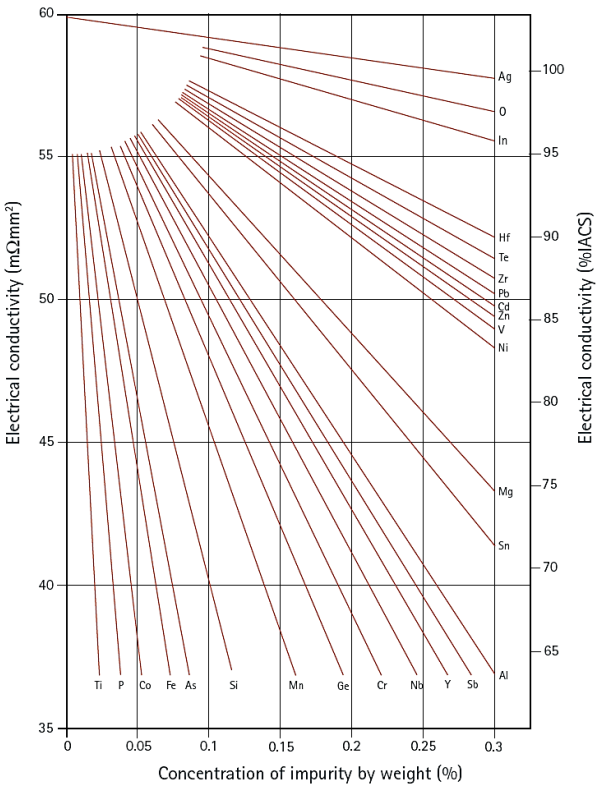

Figure 9: Effect of various elements on the conductivity of copper [34]

b) Thermal Conductivity – Thermal Diffusivity

Thermal conductivity and diffusivity, two sides of the same coin, govern the absorption and distribution of heat throughout a material. Respectively, these two properties dictate the amount of energy that a material can absorb, and how fast that material can distribute the energy throughout its volume. As seen in Equation 2, thermal diffusivity is directly related to thermal conductivity as it is a function of the thermal conductivity (λ) of the material, multiplied by the material density (ρ) and specific heat capacity (C_p) [35].

$$a = \lambda \rho C_p$$

Equation 2 - Thermal Diffusivity

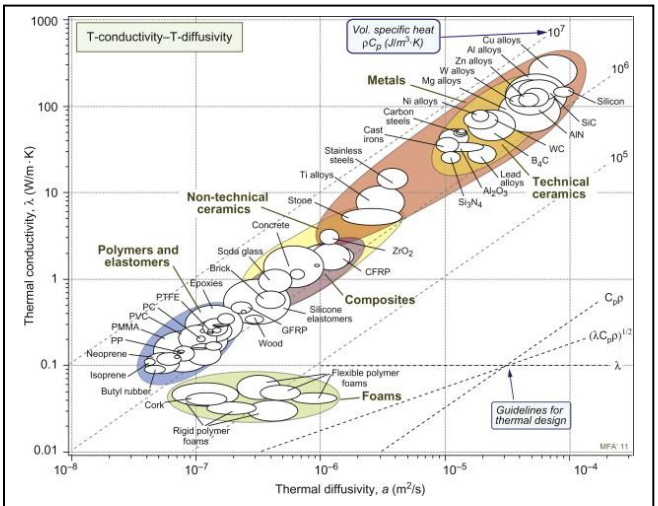

Figure 10: Thermal Conductivity vs Diffusivity [35]

Over 5 decades worth of data analysis of the thermal conductivity and thermal diffusivity show that the specific heat capacity per unit volume, ρC_p, is approximately $3 \times 10^{-6} {}^{J}/_{kg \cdot K}$ and observed to be almost constant for all solid materials. Thus, the relationship of the thermal conductivity can be approximated to be $\lambda = 3 \times 10^{6} a$, as shown in Figure 10 below [35].

Therefore, as copper and copper alloys have the highest thermal conductivity of all non-precious metals, approximately 1.67 times greater than that of aluminium and 30 times greater than stainless steel, copper is the ideal material for use in applications where high heat absorption, even distribution, and quick dissipation is required.

C. Effect on the Additive Manufacturing Process

The thermal conductivity and diffusivity of a material defines the ability that a material has, as had been mentioned earlier, been defined as the ability to absorb and disperse heat. These thermal properties can be value-added for applications where heat dissipation is required, such as in heat sinks and heat exchangers. Materials with high thermal conductivity absorb greater amounts of heat per volume and therefore would require comparatively less energy for proper layer penetration than materials with low thermal conductivity. In contrast, as the thermal diffusivity

of a material increases, so should the exposure time of the laser with the powder in order to achieve melt pool formation [36].

IX. Objectives

The purpose of this research was to explore and evaluate the value and feasibility of using pure copper as a material in metal additive manufacturing, specifically with powder-bed-fusion (PBF) technologies such as selective laser melting (SLM). By varying the laser power (P) and scanning speed (v), and keeping the hatch spacing (h) and layer thickness (t) constant, we were able to observe the effects of the AM of pure copper powder across a wide spectrum of applied volumetric energy densities (E_v). In addition to this we were able to identify the inherent challenges of using pure copper powder as a feedstock material and how they can affect the AM process.

X. Process Paramater Determiniation

The parameters used in any powder-bed fusion process can be attributed to three fundamental components, the laser, scanning strategy, and feedstock material (metal powder). Process parameters such as laser power, scanning speed, and beam width are machine-dependent and thereby controlled by the physical capabilities of the laser technology, optics, and gantry system. In contrast to this, process parameters such as the hatch spacing, point distance, exposure time, stripe width (track length), and stripe overlap are related to the scanning strategy applied and are therefore independent of the physical capabilities of the machine. A sample of this is shown in Figure 11.

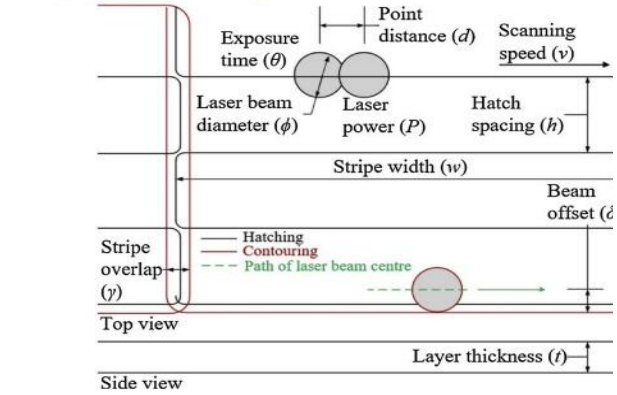

Figure 11: Illustration of SLM Process Parameters [37]

Lastly, the layer thickness used is dictated not by the machine used or the scanning strategy applied but by the feedstock material, specifically the size of the metal powder grains.

These process parameters can be further characterized by the way that they can affect the manufactured part. Laser and feedstock attributed parameters can be described as energy dictating process parameters, directly impacting the amount of energy that the material will be exposed to. In contrast, most process parameters attributed to the scanning strategy applied can be described as property-orienting parameters, as they the define the orientation of grains in the microstructure and therefore the directionality of the structural properties of the produced part.

Attributed primarily to the physical capabilities of the machine as well as the feedstock material, the primary energy dictating process parameters are the laser power ($P;\ W$), scanning speed ($v;\ {}^{mm}/_{S}$), and layer thickness ($t;\ mm$). An exception to this is hatch spacing ($h;\ mm$), which is related to the scanning strategy, and defines the space between each pass of the laser beam. The relationship between these variables can be described as the amount of energy imposed on the feedstock material per volume, or volumetric

energy density (E_V; $^{J}/_{mm^3}$) [37] and calculated through the use of Equation 3.

$$E_V = \frac{P}{v \times t \times h};\ v = \frac{PD}{\theta}$$

Equation 3: Volumetric Energy Density and Scanning Speed [37]

As seen in the additive manufacturing of Invar 36 by Yakout et al [38], the volumetric energy density applied to the powder determines the condition of the process output.

As seen in Figure 12 if this value is too low then voids and cracking can occur as a result of the incomplete melting of the powder, too high then the powder can be vaporized, and cracking can occur as a result of higher residual stresses. The point where the volumetric energy density applied results in the formation of a stable melt pool, and thereby a manufactured part with no voids or cracks is known as the critical energy density (E_C).

A. *Density, Specific Heat, and Melting Temperature*

Along with being the fundamental properties of any material, the density (ρ; $^{kg}/_{mm^3}$), specific heat (C_p; $^{J}/_{kg \cdot K}$), and melting temperature (T_m; ℃ or K) ultimately dictate the minimum amount of energy required to successfully melt the feedstock material. As seen in Equation 4, the volumetric energy to melt (E_m; $^{J}/_{mm^3}$) [37] is related to the product of the density, specific heat, and the difference between melting and ambient temperature.

$$E_m = C_p \times \rho \times (T_m - T_a)$$

Equation 4: Minimum Volumetric Energy for Melting [37]

It should be noted however, that this equation provides the amount of volumetric energy absorbed that would need to be absorbed by the material in order to achieve melting. Therefore, the

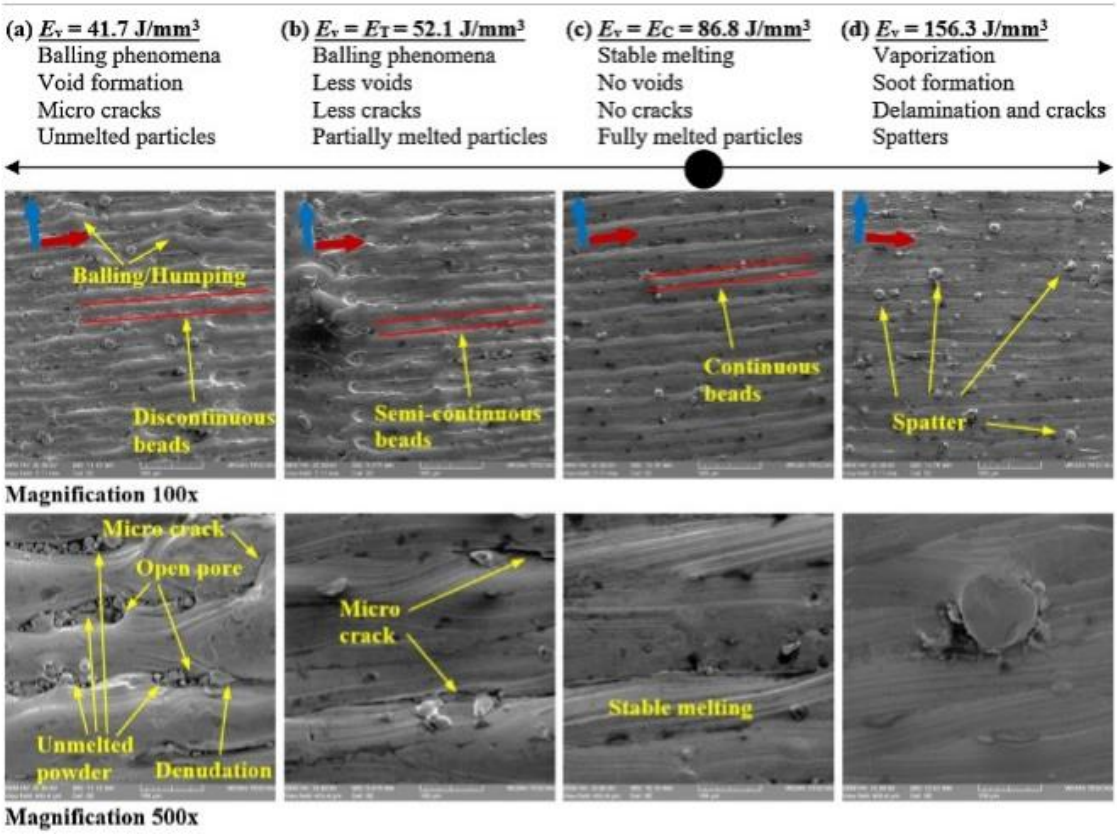

Figure 12: Microstructures of top surfaces of Invar 36 parts produced with varying volumetric energy densities [38]

volumetric energy applied to the material would need to be greater in order to account for the effect of the heat dissipation, thermal absorption, and emissivity of the feedstock material on system efficiency.

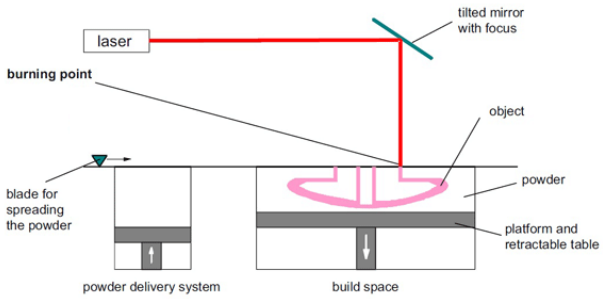

Figure 13: Illustration of a powder-bed system [56]

XI. Experimental Procedure

A well-designed experiment can substantially reduce the number of trials required. Prior to the design of experiments, extensive research was done to provide a foundation for the experiment. Additive Manufacturing encompasses defining the Process, Structure and Property (P.S.P) relationships, therefore, it is critical to have a clear understanding of how the three categories are linked and how they influence one another [39].

In the SLM process, the laser energy density involves most of the effective process parameters that affect the mechanical properties and density. When applied it can show that increasing the laser energy density increases the density and reduces the voids produced within the parts. If the volumetric energy density is too low, voids and cracking can occur due to incomplete melting of the powder. Whereas if it's too high, the powder can be vaporized resulting in cracking as a result of high residual stresses.

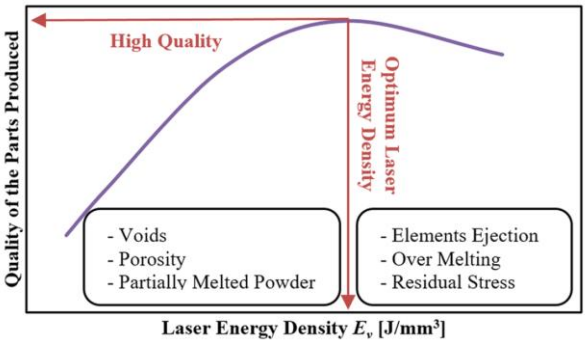

Figure 14: Relationship between the optimum laser energy density and the quality produced parts [37]

Figure 14 shows how there's an optimized range of laser energy density that can be determined for every material based on their properties and the experimental verification. When the applied volumetric energy density leads to the formation of a stable melt pool, and thereby the manufactured part has no voids or cracks, it is known as the critical energy density, E_c.

As can be seen in Table 3, the properties of the typical alloys that have been processed in AM are very different from Copper's properties, specifically when considering the conductivity and diffusivity. Therefore, it was necessary to design an experiment to analyze the effect of the process parameters on the resulting properties, microstructure, and density of a manufactured sample.

Material	Specific Heat (J/kg*K)	Density (kg/m³)	Conductivity (W/m*K)	Diffusivity (mm²/s)
Copper	376.812	8940.00	395.00	117.26
SS 361L	468.00	8000.00	16.30	4.35
Inconel 617	419.00	8360.00	37.10	10.59
Titanium	544.28	4500.00	25.00	10.21
Aluminum	1080	2385	94.03	36.51

Table 3: Common AM materials compared to Copper

A. *Factorial Design of Experients*

As in the various studies referenced throughout this report, a design of experiments (DOE) was developed in the interest of narrowing down a combination of process parameters that would produce parts with mechanical and electrical properties closest to other manufacturing processes. In the interest of time, and "coverage", a two factor – four level DOE was used with the hatch spacing and layer thickness set as constant variables, and laser power and scanning speed as control variables. This resulted in a total of 16 unique variable combinations.

B. *Parameter Identification*

Most of the research available in open literature focuses on the optimization of process parameters using electron beam manufacturing (EBM), which will be seen at Lodes et al. However, EBM has a larger spot size when compared to SLM which can be a problem if finer features are required to be produced. Furthermore, there are only a couple of studies done on pure Copper. Most of the research involved Cu-based processes which employed the alloys rather than Copper only. The next few sections will summarize the work of each literature to provide a comparison of the different methods used.

1. El-wardany et al

The deposition of OFHC via laser additive manufacturing (LAM) is not as advanced as EBM due to its high reflectivity and high thermal conductivity [28]. These properties can contribute to solidification cracking and porosity when depositing Copper using LAM. These kinds of defects could be due to powder particle morphology, insufficient energy and thermal history. It was therefore concluded that for LAM high laser power and Low deposition scan speeds are required in order to successfully deposit pure Copper without compromising the physical and mechanical properties of Copper [28]. Below are the challenges with different approached to overcome them.

The high levels of porosity that were observed in the resulting builds were a result of the residual oxides that are both internal and on the surface. Another main issue of the presence of oxide layers is a significant decrease in the electrical conductivity of copper. This can have a big impact on any electrical applications. In order to minimize the internal oxidation, the powder production process should be done with an inert gas atomization to have negligible interior oxygen content. As for the surface oxides, there are three suggested ways to minimize them:

1. Use of reducing gas environment during the AM process: This strategy employs reducing gas in the system to allow for the powder carrier gas to be fed from a pre-mixed gas cylinder of 4% hydrogen in Argon forming gas.
2. Use of an alternative Copper alloy to reduce the sensitivity to oxides: The addition of alloying elements to Copper was investigated to eliminate the porosity caused by Copper oxide. However, the use of an alloy can degrade the conductivity of Copper which is why the selection process must be done properly [28]. Figure 15shows the effect of alloys on the conductivity of Copper. The three materials with the least detrimental to conductivity are Silver, Cadmium and zinc. In this paper, they used 3% zinc-Copper powder and the results showed 97% conductivity with reduction in internal porosity.
3. Protection of powders: An effective solution to reduce the oxide formation is the treatment of the copper powder to ultimately coat the reduced powder by a thin layer of Polydimethylsiloxane (PDMS) which will vaporize away before the copper powder reaches the melt pool during the DED process. The results showed an improvement in the

quality of the copper deposits.

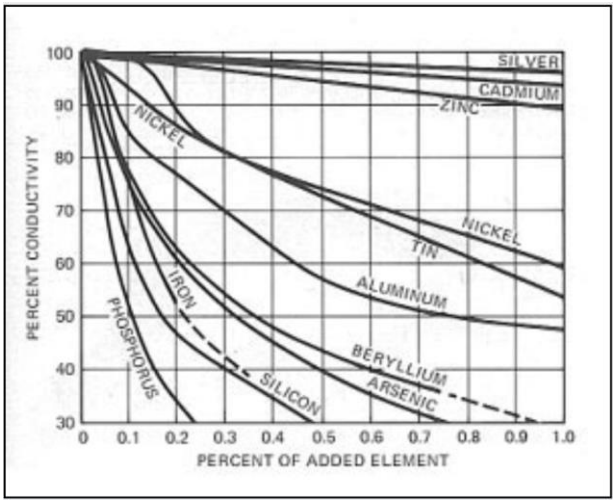

Figure 15: Influence of alloying elements on Copper conductivity

The focus of the El-wardany paper was the DED process, which is not what this report entails. However, the development that this paper had for the powder bed process involved building Copper on Steel substrate as well as on the Copper substrate. A single-track melt pool model was developed, and the results showed temperature distribution in the powder and substrate to predict the process parameters. With a laser power of 180W and scanning speed of 2800mm/s the modeling results obtained showed a porosity of ~ 18% (or 82% density). This was used to create DOE with a goal of increasing laser power and volumetric energy density [28].

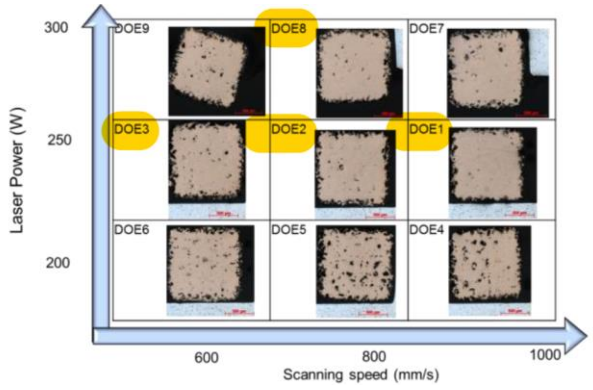

Figure 16: The DOE with the parameters chosen [28]

Figure 16 show transverse cross section of the Cu on Copper substrate specimens. The observations on the results confirm that increased power is effective at reducing porosity. On the other hand, the effect of the scanning speed is not as apparent. When the specimens were examined in the longitudinal direction it was evident that the amount of lack of fusion decreases with increasing melt pool size. Some samples showed a few spherical powers which are typically associated with gas evolution.

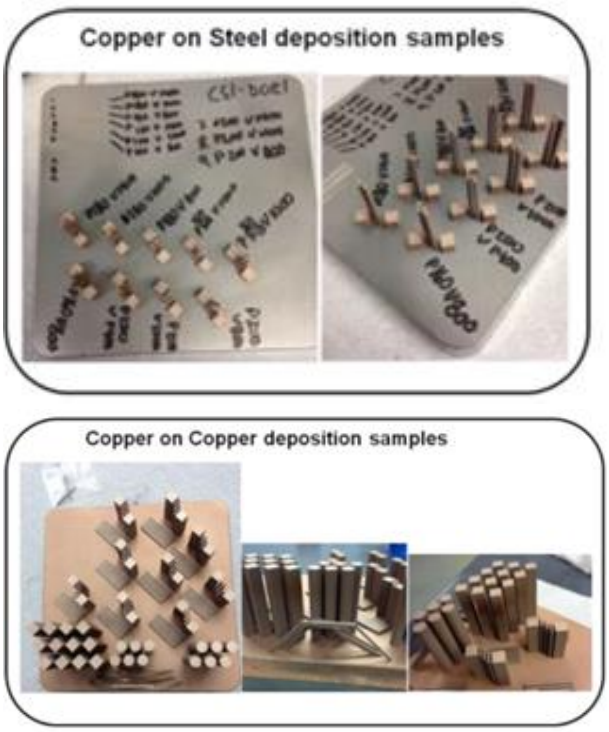

Figure 17: Copper samples built on Cu substrate on left and on Steel substrate on right [28]

Figure 17 show the Copper specimens on both the Copper substrate as well as the steel substrate. The electrical conductivity for the specimens built on the steel substrate showed a lower conductivity. This is due to iron diffusion in the copper build from the steel substrate. Furthermore, when measurements were done to assess the impurities in the powder, it was found that there was 0.6% Phosphorous. This can have a drastic reduction in the electrical conductivity which means that there must be a higher control of

the amount of impurities that can be present during the powder production.

The experimental results show that the maximum density obtained was ~91% which should that there is good correlation between the model predicted substrate melt pool size and the measured density. This is shown in Figure 18which also show that the measured densities have a strong correlation with the volumetric energy density.

up to 1000mm/s, the laser beam is 35µm and layer thickness can vary from 20-100µm. The Copper powder particle shape and size distribution was good as the powder was obtained through gas atomization. Different process parameters were used (as shown in Table 4 below) whereas the layer thickness and hatch spacing were fixed at 50 µm and 0.12mm respectively [40].

The results obtained showed successful

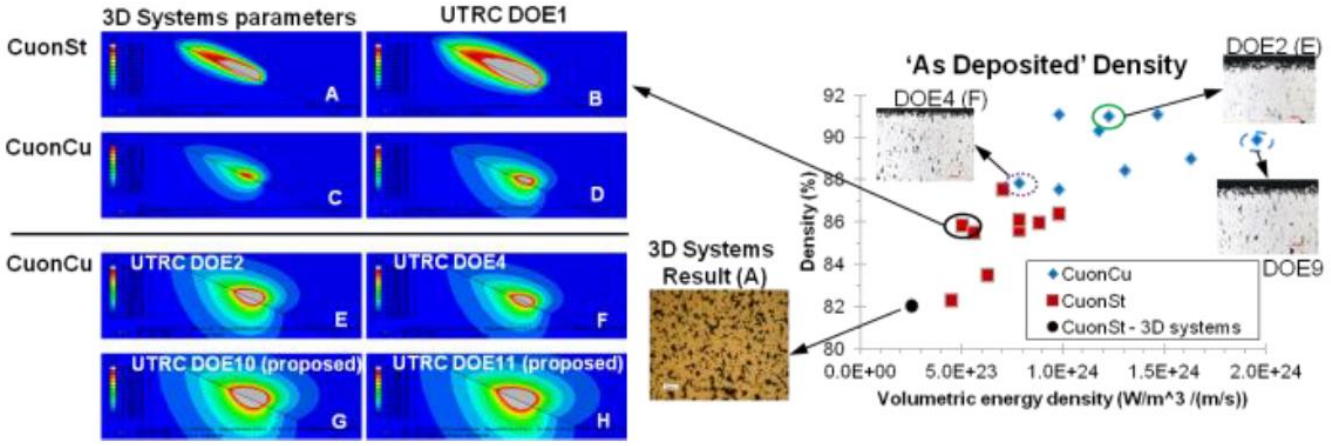

Figure 18: Melt pool model results (left) and measured densities of samples as a function of volumetric density (right) [28]

2. Lykov et al

According to Fraunhofer Institute for Laser Technology, researches minimal laser power for successful SLM of copper should not be less than 300W [40]. Some studies used powers that reached 1000W, however, not all machines have those capabilities. Lykov et al used a SINTERSTATION Pro in the research which allows a maximum output power of 200W. The scanning speed can go

build with a good dense structure and good surface finish quality without any dimensional distortions as shown in Figure 19. According to the analysis of the samples obtained, 1 showed the highest porosity whereas 3 showed the lowest porosity.

The volumetric energy was calculated for each sample and sample 3 had the lowest E_v of 133J/mm^3, whereas 1 had an E_v of 267J/mm^3

N of specimen	Laser power, [W]	Scanning speed, [mm/s]	Point distance, [µm]	Exposure time, [µs]
N1	200	100	50	400
N2	200	150	50	400
N3	200	150	100	400
N4	200	100	50	400
	100	200	200	200
N5	200	100	50	400
	150	300	300	100

Table 4: SLM process Parameters

Figure 19: Copper specimens produced by SLM [40]

The tensile strength achieved from specimen 1 showed to be 149MPa. This value compared to one of wrought copper to be 221-379MPa shows low.

3. Zhang et al

Due to the high conductivity of Copper and therefore its alloys, most of the laser energy will be easily lost to the surroundings (particularly the dense substrate) which can result in partial or no melting [25]. This causes the melt track to become unstable and discontinuous along with potential balling effect that can take place (due to surface tension in molten state), the densities of the copper parts produced are less than 95%. This study used SLM250HL to build C18400 Copper alloy (chemical composition shown in Table 5). The machine has two laser types, one of Gaussian beam with maximum power of 400W and focus diameter of 80 μm and a uniform beam profile with maximum power of 1000W and focus beam diameter of 730 μm. The copper powder was produced by gas atomization with an average particle size of 12 μm.

Cu	Cr	Si	Zr	Fe	Others
98.37–98.12	0.5–1.2	<0.1	0.03–0.3	<0.08	<0.2

Table 5: The Chemical composition of C18400 [25]

The layer thickness was fixed at 50μm whereas the hatch spacing for Gaussian laser was from 0.05mm to 0.15mm and in the uniform laser from 0.1mm to 0.2mm.

Scan speed (mm/s)	Laser power(W) 200	300	400
100	S10	S11	S12
600	S20	S21	S22
1000	S30	S31	S32

Scan speed (mm/s)	Laser power (W) 200	400	600	800	1000
100	S13	S14	S15	S16	S17
600	S23	S24	S25	S26	S27
1000	S33	S34	S35	S36	S37

Table 6: Process parameters for Gaussian and for uniform laser [25]

The results obtained are shown in Figure 20. Since the focal diameter of the uniform laser is almost 9 times larger than the gaussian laser source, the energy input during manufacturing will be 9 times smaller under the same laser power input. There are three main ways to characterize the melting surfaces:

1. Insufficient laser energy input causing discontinuous melting and lack of fusion. For uniform laser, power less than 200W and speed higher than 600mm/s had that.
2. Complete melting where continuous and dense surface was obtained with laser power 400W to 1000W combined with scan speed 600mm/s to 1000mm/s as for the gaussian laser, laser power from 200-400W and scan speed larger than 100mm/s,
3. Overheating was a result of using large energy input resulting in severe evaporation and oxidation of the specimens.

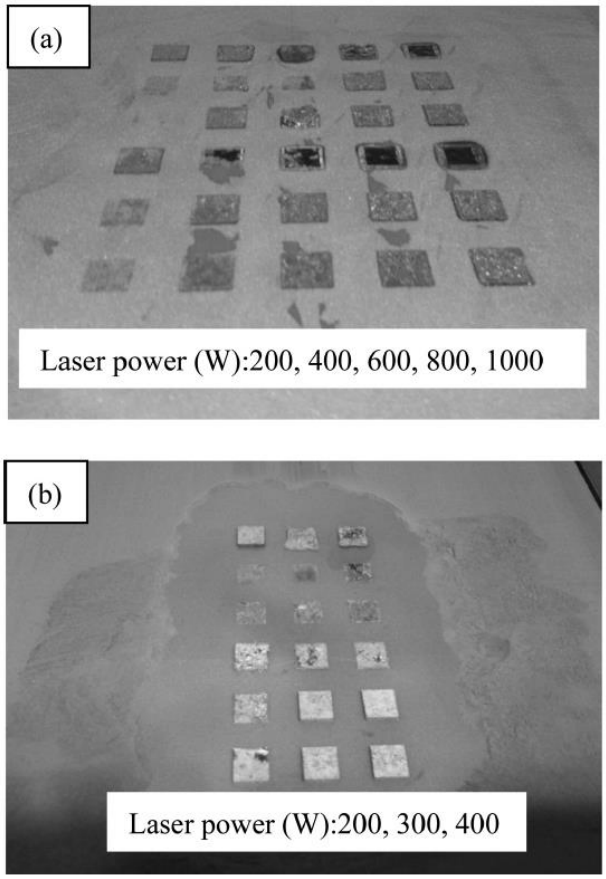

Figure 20: Surface of C18400 using parameters set in Table 6

a. Uniform distribution laser,
b. Gaussian laser source [25]

When some of the SLM samples were examined, it was clear that the amount, size and shape of porosity were associated with the laser input conditions. This proved that the laser energy input can help the densification of the powder system. The measured relative density was 92.99%. Figure 4.3.4 shows the porosity of the SLM samples using optical microscope under different forming parameters. It was evident that the amount of porosity, the size and shape of pores were associated with the laser input conditions [25]. This demonstrated that sufficient laser energy input can benefit the densification behavior of the powder system. The measured relative density of the SLM sample was 92.99%. However, under the same condition, further decreasing scan speed from 300 mm/s to 100 mm/s (as shown in Figure 21c), the as built specimen showed enlarged pore size up to 100μm. This was a result of overheating during the melting process which caused copper material to evaporate. Under uniform distribution laser source, as shown in Figure 21d, the amount of pores decreased compared to Figure 21b. This was due to the uniform distribution of laser source which compensate the large thermal conductivity of Cu powder by applying laser input without deceasing powder from laser beam center to the edge. The measured relative density was 96.74% [25].

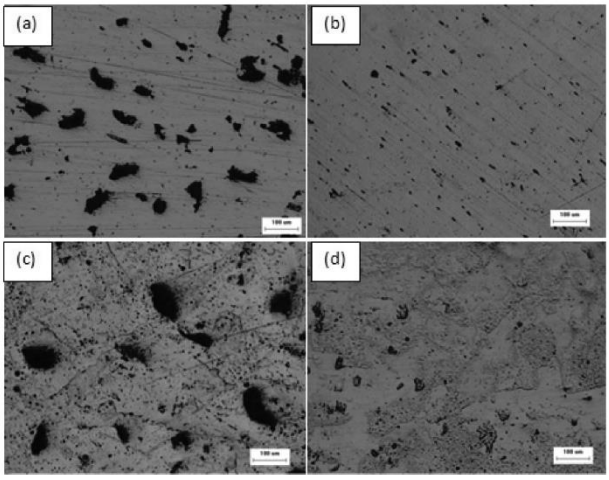

Figure 21: Images of SLM Cu based samples:

(a) P= 300W, v= 600 mm/s, h =0.15 mm,t= 0.05 mm.
(b) P= 400W, v= 300 mm/s, h= 0.15 mm, t= 0.05 mm.
(c) P= 400W, v= 100 mm/s, h= 0.05 mm, t= 0.05 mm.
(d) P= 800W, v= 600 mm/s, h= 0.10 mm, t= 0.05 mm. [25]

4. Scimmarella et al

Th work presented in this paper showed that it was possible to build a 12 cubic mm volume of C1100o Copper onto a 4142-steel substrate. The process developed in this study was focused to maximize the deposition efficiency which is defined as achieving a relatively stable melt pool and able to deposit several repeatable layers. This study utilized an Optomec LENSTM 850R system which is a DED process.

Method	Power, W	V, mm/s	pfr, g/min	Layer thickness, mm	Spacing, mm
Control	900	2.1	1.6	0.25	0.50
Process (I)	900	2.1	3.3	0.75	1.50
Process (II)	990	2.1	3.3	0.75	1.50

Table 7: Process parameters used during C11000 deposition [41]

Table 7 shows the process parameters used. The corresponding deposition rates of the Control, Process (I) and Process (II) were 0.14, 1.25 and 1.55 g/min respectively [41]. In order to improve the deposition rate, the thermal energy was added to the substrate to increase the heat input. The heat required for melting a given volume of copper metal was estimated using:

$$Q = \rho C_p(T_m - T_0) + L$$

Equation 5: Minimum Volumetric Energy for Melting [41]

where ρ is density (g/cm3), C_p is heat capacity (J/g-K), T_m is the melting temperature (K), T_o is the initial temperate of the substrate (K)and L is the latent heat of fusion. The value of Q represents the minimum energy required for stable melting. So, if T_0 is higher than room temperature at the beginning of the process, then the energy contribution by the laser per unit length, given as $H_{ln} = P/V$, is required to push the total energy above the threshold Q for melting.

Based on the absorptivity calculations for copper, the % of energy absorbed is near 10% at room temperature for a laser wavelength of 1.06μm [41]. This quantity will increase to 25% as the temperature of the copper approaches its melting temperature. Furthermore, the high reflectivity of copper makes it so that nearly 75% of the energy is reflected when the temperature of Copper is at its melting temperature. Furthermore, near $0.9T_m$ of pure copper, the thermal conductivity decreases to 340W/m-K. This in turn allows for more energy absorption at the beam/workpiece junction. As the heat capacity increases with temperature, the thermal conductivity decreases, therefore, energy absorption will increase as the temperature increases. The aim of this study was to ensure that enough thermal energy into the build to encourage continuous deposition of the C11000 powder into the melt pool that forms on the surface of the copper deposit [41].

5. *Lodes et al*

Although this research paper works with pure Copper, it uses EBM. The advantage of using SEBM is that it is not influenced by optical reflectivity of materials and it offers high potential for the processing of pure copper. It also has another advantage in which it inhibits oxidation as the process is conducted in vacuum [42]. This study focused on developing the process for the SEBM manufacturing of 99.94% pure copper on the basis of the correlation of process parameters and porosity. The copper powder used was gas atomized with a particle size of 45-106 μm. Table 8 shows the process parameters used. Compared to the usual materials manufactured by SEBM, pure copper had a high thermal conductivity. Initially it

Temperature	400 °C
Chamber pressure	2×10^{-3} mbar (Helium)
Voltage	60 kV
Beam current	5–42 mA
Beam velocity	2000–10,000 mm/s
Line offset	0.1 mm
Layer thickness	50 μm

Table 8: Process parameters applied for sample production [42]

was a concern how the fast heat dissipation can make it impossible to sustain the desired build temperature. However, the heat flux is dominated by the bad thermal conductivity of the powder bed itself.

The process is illustrated as a range of line energy E_i and beam velocity v in which dense parts with good surface quality can be produced. The line energy correlates beam velocity ν and power P of the electron beam is the product of voltage U and current I.

$$E_i = UI/\nu$$

Equation 6: Line energy affecting heat flux [42]

When too little energy is supplied, not all of the powder will melt which will lead to layer defects and porous components. On the other hand, too much energy input typically leads to swelling which occurs mostly at edges of samples due to local overheating. Moreover, balling effect can occur forming melt droplets on the surface due to the surface tension of the molten metal [42].

The results show that the samples are denser with higher line energy for all beam velocities. In Figure 22, the first sample with line energy of 0.15J/mm is not dense and shows porosity. The surface is typically matte and lots of binding defects can be seen in the micrograph. This proves that some regions are not completely melted as energy input was too low. The second sample with line energy of 0.3J/mm is a dense part with no binding defects. The surface is slightly shiny with typical SEBM melt tracks. The last sample shown with a line energy of 0.35J/mm was built with too much energy input which led to swelling.

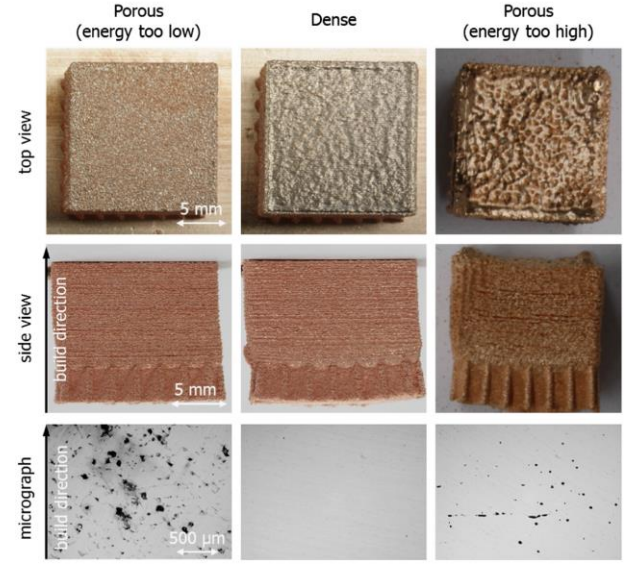

Figure 22: Showing micro and photographs of the samples as builds by different line energies [42]

From left to right,
0.15J/mm, 0.3J/mm and 0.35J/mm

The very shiny surface does not show melt tracks but rather upward bending of the edges. The side view of the sample shows overheating as some of the copper powder sticks to the melt surface during raking which leads to porous areas and binding defects.

C. *Constant Variables*

In the interest of time the layer thickness and hatch spacing were designated as constant variables set for the copper DOE, set to 40 µm and 110 µm respectively.

As the layer thickness of a manufactured sample is dependent on the quality of the feedstock material, an experiment analyzing its effect would require multiple prints. Which, due to the lack of consistency between prints even at constant parameters, would result in unreliable data. Therefore, the value was set to 40 µm as a result of the particle size distribution of the material used.

Hatch spacing is a parameter related to the scanning strategy applied and is therefore independent of the feedstock material used. Despite this, it was designated as a constant

variable in the pilot experiment as, in comparison to the scanning speed or laser power, it has a limited effect on the resulting energy density applied. In addition to this, adding the hatch spacing as a third control variable would increase the complexity of the DOE and thereby the time required for processing and analysis. Therefore, the value was set to 110 µm, 30 µm greater than the laser beam size of 80 µm, thereby eliminating any overlap in beam passes and limiting the overlap of the melt pool.

D. Control Variables

The control variables designated in this experiment were the laser power and scanning speed, both parameters that are independent of the feedstock material and therefore can be altered for each sample in a single print. Their ranges were set to 90 – 135 W and 300 – 330 mm/s respectively.

Defining the amount of energy applied to a material per second, the laser power was chosen a control variable due to the significance of its impact on the resulting energy density, see Equation 3. As noted in Thermal Conductivity – Thermal Diffusivity and Table 3: Common AM materials compared to Copper, as a result of the high thermal conductivity of copper the magnitude of laser power required would be relatively low as compared to what is commonly used in the printing of parts using stainless steel 316L. This is due to the significantly higher rate of absorption of thermal energy found in copper than that of steel.

Defining the length of exposure time of the energy applied to the feedstock material, the scanning speed was selected as the second control variable also due to its impact on the resulting energy density and the degree to which it can be manipulated. As noted in section **Error! R eference source not found.** and **Error! Reference source not found.**, as a result of the high thermal diffusivity of copper the variable range is relatively low as compared to the scanning speed used in the printing of parts using stainless steel 316L as the feedstock material due to the higher rate of dispersion of the thermal energy applied throughout the material and therefore the increased amount of time that would be required for the target area to reach the desired temperature.

The range of both parameters was selected such that the corresponding minimum energy density at least met E_m with the maximum not exceeding E_b. In addition to this the values were set such that there is a relatively significant step-size between each level of laser power and scanning speed, 15 W and 30 $^{mm}/_{s}$ respectively, thereby, enabling a more effective observation between the effect of the individual parameters on the resulting properties of the produced samples.

It should be noted that, though some power/scan speed combination can have similar volumetric energy density, the resultant output is not necessarily identical. At different power and speed, the solidification process, and therefore the resulting microstructure of the material, will be different and can yield favourable or undesired results [43].

Efficiency		V_{scan} $^{mm}/_{s}$							
Est.	76.25%	**300**		**330**		**360**		**390**	
Power (W)	**90**	1564.29	51.99	1423.99	47.26	1307.07	43.32	1208.14	39.99
	105	1821.50	60.65	1657.82	55.14	1521.42	50.54	1406.00	46.66
	120	2078.71	69.32	1891.65	63.02	1735.76	57.77	1603.86	53.32
	135	2335.93	77.98	2125.48	70.89	1950.11	64.99	1801.71	59.99
		(ºC)	(J/mm^3)	(ºC)	(J/mm^3)	(ºC)	(J/mm^3)	(ºC)	(J/mm^3)

Table 9: DOE Control Variables with predicted melt pool temperature and energy density at 76.25% EAE

E. *Effective Energy Absorption*

As discussed in Process Paramater Determiniation, the end process parameter of any metal additive manufacturing process, volumetric energy density represents the amount of energy per volume, Equation 3: Volumetric Energy Density and Scanning Speed. However, as this formula is a function of laser power, hatch spacing, layer thickness, and scanning speed (i.e. inherent machine related properties), it does not necessarily represent the energy per volume absorbed by the powder as it does not account for the effect of thermal conductivity and diffusivity, as well as the effect of powder morphology and emissivity. Additionally, as these variables are related strictly to the feedstock material, and therefore independent of the equipment used, their effect on energy absorption efficiency (EAE) can be attributed as material/product property.

F. *Effect of Emissivity*

The emissivity of a material is the measure of the percent thermal absorption. Therefore, in the case of copper, whose emissivity 0.05 when polished and 0.15 when molten [44], it is theoretically safe to assume that the emissivity observed is closer to its molten state as the polished unmolten state is only true at the initial instance of exposure. However, the emissivity alone would not provide an accurate estimate of the efficiency of energy absorption as only a fraction of the thermal energy reflected does not radiate to another particle (specifically 25 percent, as angle of reflection of beams perpendicular to the center of a sphere is less than 90 degrees, up to r/2 from the center).

Therefore, assuming perfect particle distribution, this means that for 75 percent of the surface of the powder particle the effect of emissivity is negligible as the reflected thermal energy reflects between it and the neighboring particles. Resulting in an estimated impact on efficiency of $0.75 * 1 + 0.25 * 0.15 = 0.7875$ *or* 78.75% for pure copper powder.

XII. Observations

There have been some advancements to overcoming the challenges that come along with copper. Therefore, based on the research that was done prior to starting this project, the following strategies were implemented: electrochemical copper plating, build plate heating, increased cooling time, powder sieving, and recycling.

A. *Electrochemical Copper Plating*

Half of the substrate was electrochemically copper coated to replicate the findings of El-wardany et al, who had found that copper parts printed on a copper substrate had greater density relative to parts printed on a steel substrate. The substrate therefore consisted of a 1-inch thick stainless-steel plate with a 40-micron coating on on half the plate.

Figure 23: Copper plated substrate (left)

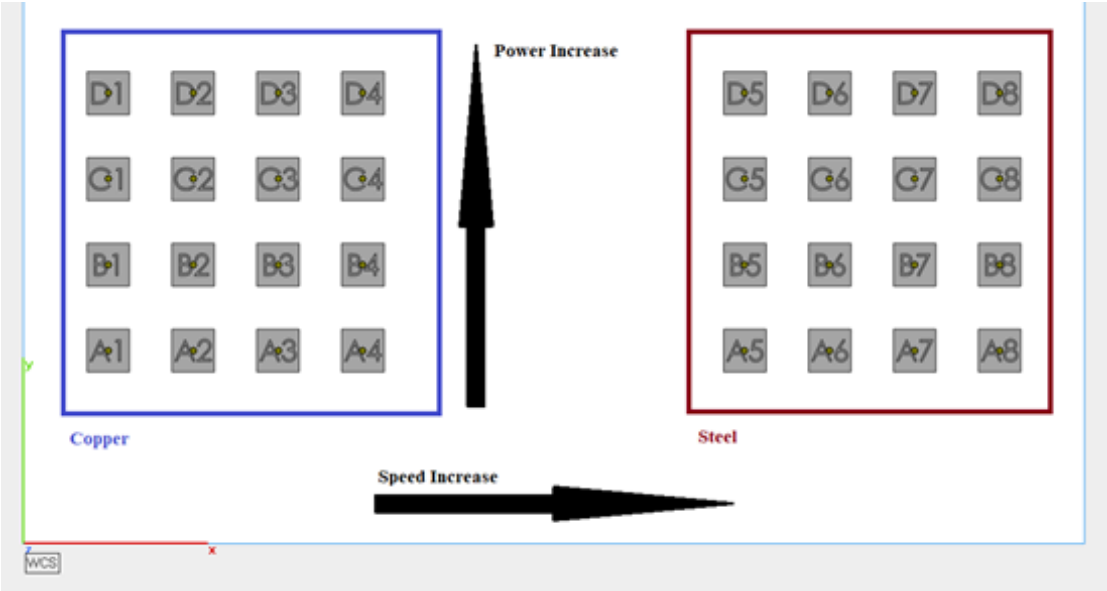

Figure 24: Parts Layout

B. *Buildplate Heating*

As the general findings by Yakout et. al. has been that there is a reduction in latent stressors when baseplate heating is maintained, thereby giving an increase in density, the parts were printed on a sustained substrate heat of 200°C.

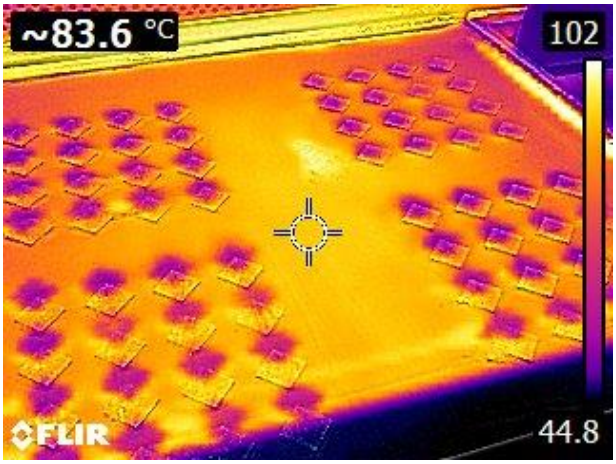

Figure 25: Localized Heating Areas

NOTE: Image taken through IR filtering glass. Large filtering occurring and therefore temperature is not accurate.

C. *Part Cooldown*

As parts were experiencing breakage with the recoater movement, a deduction was made that the parts required more cooldown time between each layer as large temperature spikes could be seen in the localized areas using thermal cameras. As a result, each part was duplicated and settings applied with 0W exposure, effectively creating ghosted parts.

Figure 26: Part Breakage

D. *Powder Handling*

1. *Loading*

The powder was loaded as a block and then sieved in order to break apart the wetted powder. Powder was handled using gloves as the raw material was sharp and caused several red spots on exposed skin during handlings.

Figure 27: Initial Powder Block

2. *Recycling*

During the sampling, to facilitate rapid oxidation, the powder was reused and sieved multiple times during the print. A total of 3 sieves were done and several colourations of powder was observed.

Figure 28: Multiple Oxidation States Exposed

E. *Part Oberservations*

3. *During Printing*

During the manufacturing process, there were several unique occurrences when compared to a steel series-based material like stainless steel 316L in that the copper powder readily oxidized even though it was in a nitrogen-based atmosphere with as little as 0.29% oxygen. As can be seen in Figure 29, there was visible oxide layers being formed as the parts was printing while also showing a clear line where the copper plating started. It should also be noted that the oxidation streaks were primarily in the steel substrate part of the build plate and can be used as an indicator that there should be differences in the part's overall density and stresses when the process is finished.

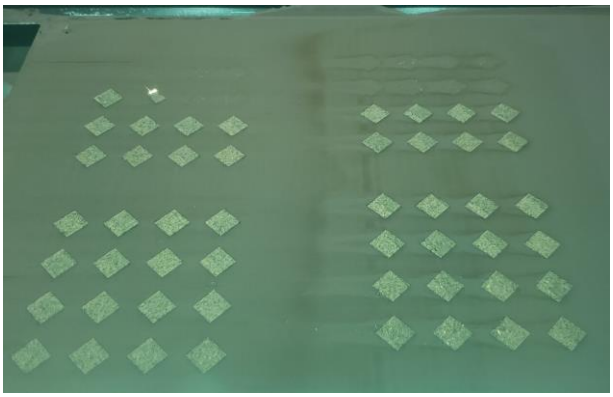

Figure 29: Oxide streaks on top layers

Using high speed imaging, throughout several observations, it was noted that the amount of spatter that occurs during the printing process of copper is significantly less with only a couple of instances found during the recordings. With Figure 30 as a sample of spatter formation, it can be noted that only a small part of spatter is formed before quickly cooling down as the laser continues to move. Each picture in Figure 30 is separated by $2/1024^{th}$ of a second and is in focus during the laser pass by. Later visual observations confirmed that spatter formation was minimal throughout the process, however, this might also be due to the incomplete melting of the powder as discussed in the Scanning Electron Microscope section.

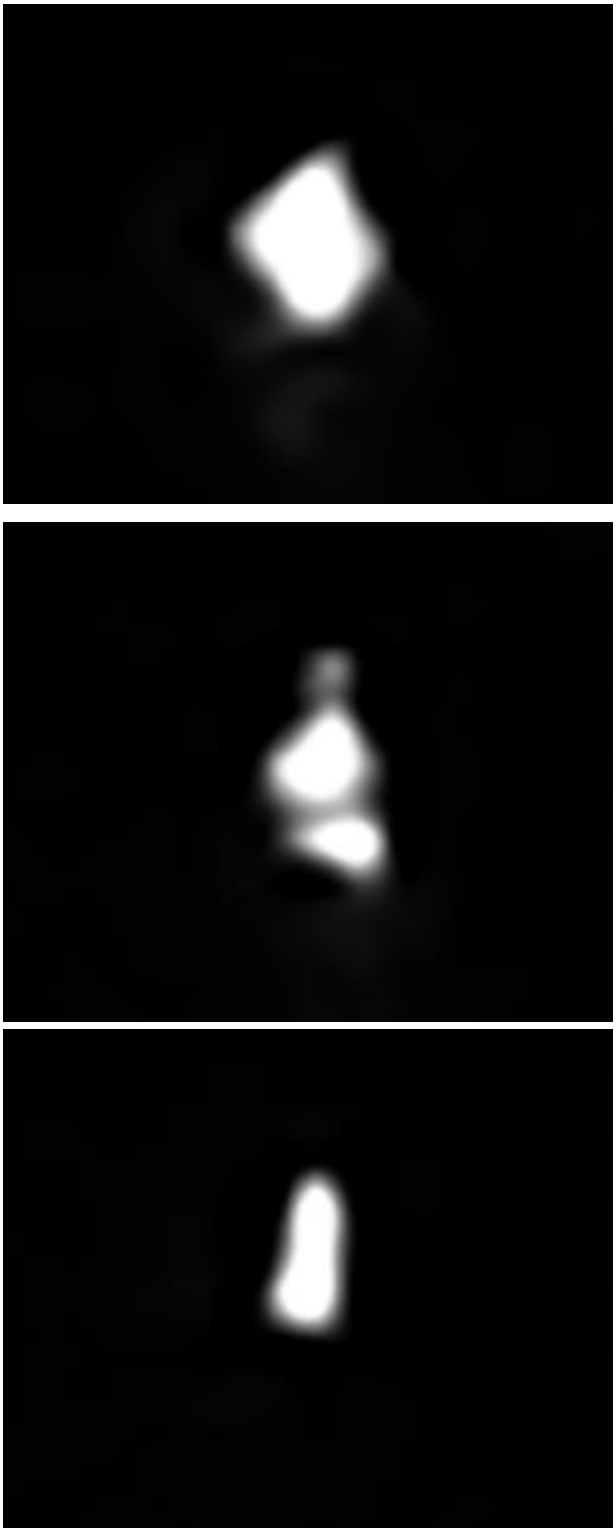

Figure 30: High-speed observation of spatter

4. On Substrate

After part extraction, several broken parts were observed whereas the energy duplicates did not break that was located on the steel substrate. As the energy duplicates were intact, this was attributed to the recoater impacting and not an indicator of the parts strength.

Once the powder was cleared from the substrate, clear layers became visible indicating each of the recycling steps and sieving operations done. Each of these layers corresponds to a specific oxidation state of copper and is reflected as such in the part analysis.

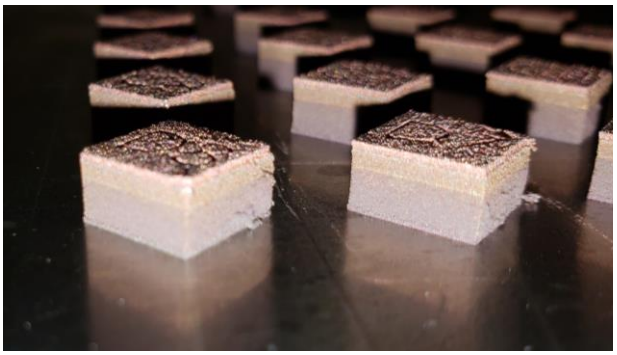

Figure 31: Visible layers after cleanup

Immediately following part extraction, the surface finish was rough to the touch and some sharp edges were observed in the part as can be seen in Figure 32.

Figure 32: Parts after extraction. Notice rough surface texture.

As seen in Figure 33, the surface roughness is far from desirable, however, it should be noted that no surface finishing operations were done on the part with secondary or tertiary exposures at lower power levels to facilitate a smoother surface. Therefore, future optimization can be done for this problem.

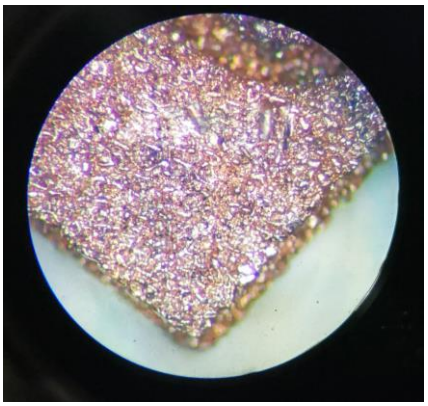

Figure 33: Microscope enhancement of part surface

XIII. Analysis

Through the analysis, the parts with the highest, lowest and median power were analyzed for density, stress and composition. As these samples were analyzed, some analysis will not include results from those units as they were destructively tested and could therefore not be used in further analysis, though a secondary pair that was printed with similar power will have results.

A. Scanning Electron Microscope

Using the Scanning Electron Microscope (SEM), several key points can be observed that is not visible by both touch and regular microscopy.

Looking at the scales of power for the parts produced on the steel side, from minimum to maximum, ref. Figure 34, with low power, large discontinuous beads form with lots of balling and several voids. These effects are clear indicators of incomplete melting and large reduction in part density, strength, and conductivity; thus, this is the most undesirable effect and should be avoided in the future. Within the middle range, there is already a great reduction in voids though balling still occurs and is significantly reduced in size. This would still be considered undesirable but are early indicators that power has a large effect on the parts even though through calculations, the part should have experienced complete melting. Finally, looking at the maximum power part, this part shows the start of semi-continuous beads and is therefore the closest to what is desired in AM. Further expansion towards this power scale should be used in future projects with SLM and nitrogen based environments.

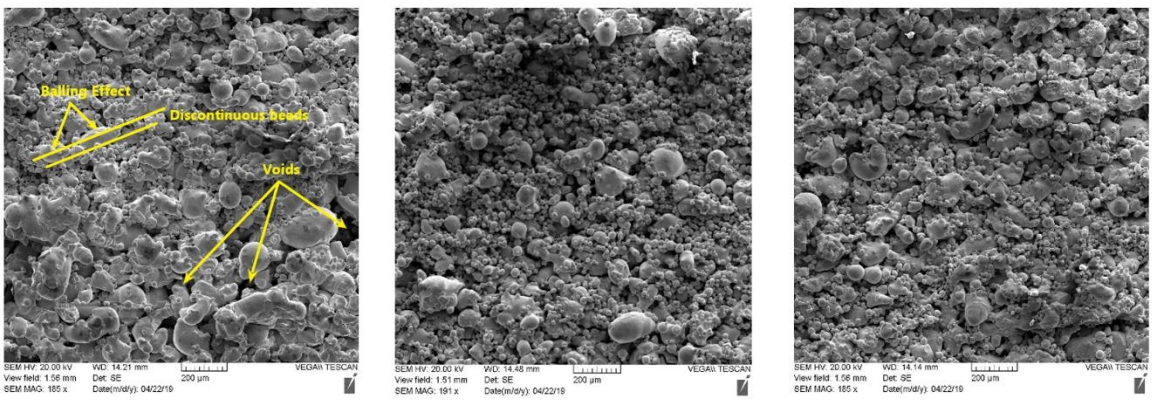

Figure 34: SEM micrographs showing microstructure of top surface of Pure Copper at different energies

a. *Sample B5* =60.65 J/mm^3 b. *Sample D8* =59.99 J/mm^3

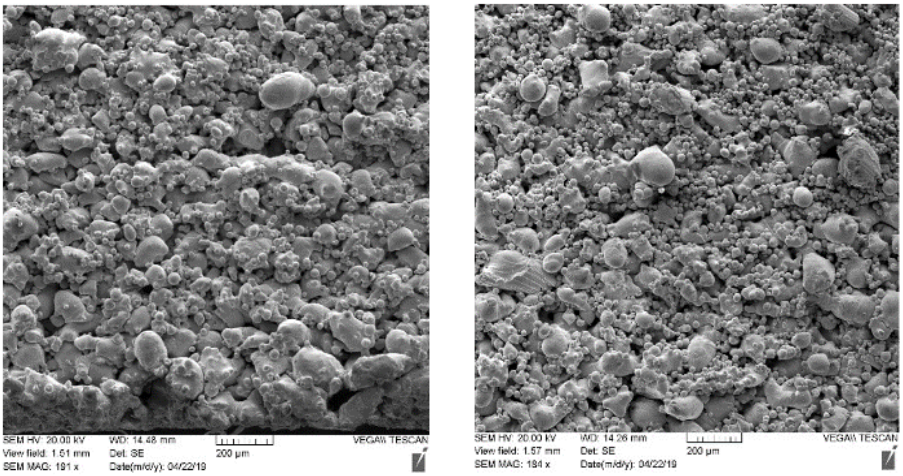

Figure 35: SEM micrographs showing microstructure of top surface of Pure Copper at ~60J/mm3

Observing Figure 35, with parts that are almost equal in power, a noticeable decrease in voids is a reduction in globule size. This could be attributed to a difference in the power and velocity as these samples were both on the steel substrate.

As a test for double exposure to facilitate further densification, parts C4 and C8-1 were used as energy doubles with part C8 experiencing a second exposure at the same power during each layer. In both C4 and C8-2, large voids can be noticed and big globules throughout, while C8-1 with a double exposure has smaller globules and voids throughout with some indications of beads forming. Therefore, further tests should be done with the determination of the residual stresses to determine if this is a viable strategy in developing high conductivity, high reflectivity parts.

Finally, when looking at the layers from the top, bottom and middle where several different levels of oxidation occurred, as seen in Figure 37, the globules at the bottom layers show much smaller sizes and much less voids than that of the top layers. These images also indicate that through the increase of power, cleaner sides can be observed and therefore can be a use case if side finishing is required alongside double exposure.

a. Sample C4 on Copper plated Steel *b. Sample C8-1 on Steel w/Double exposure* *c. Sample C8-2 on Steel w/single exposure*

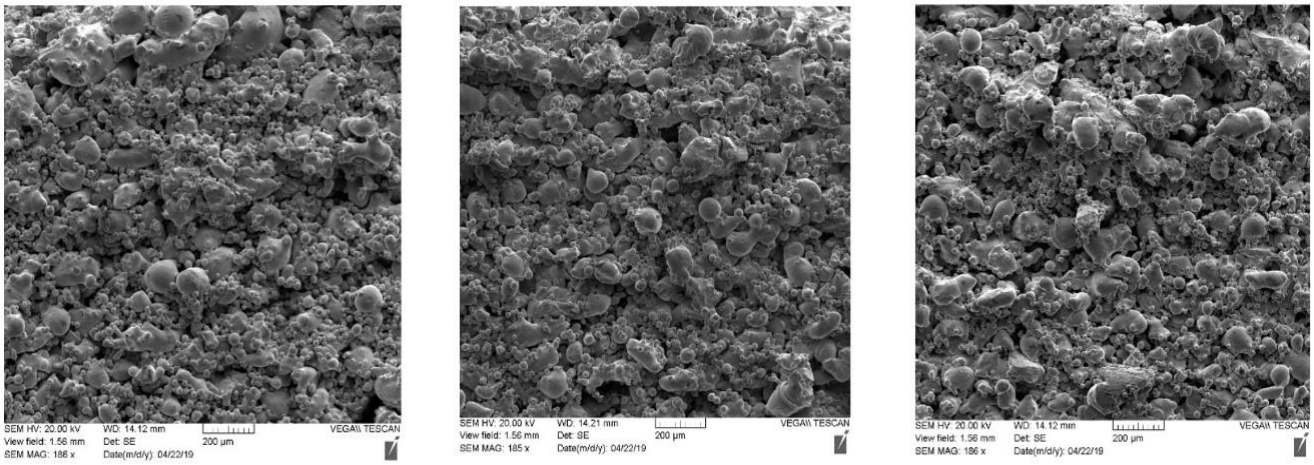

Figure 36: SEM micrographs showing microstructure of samples

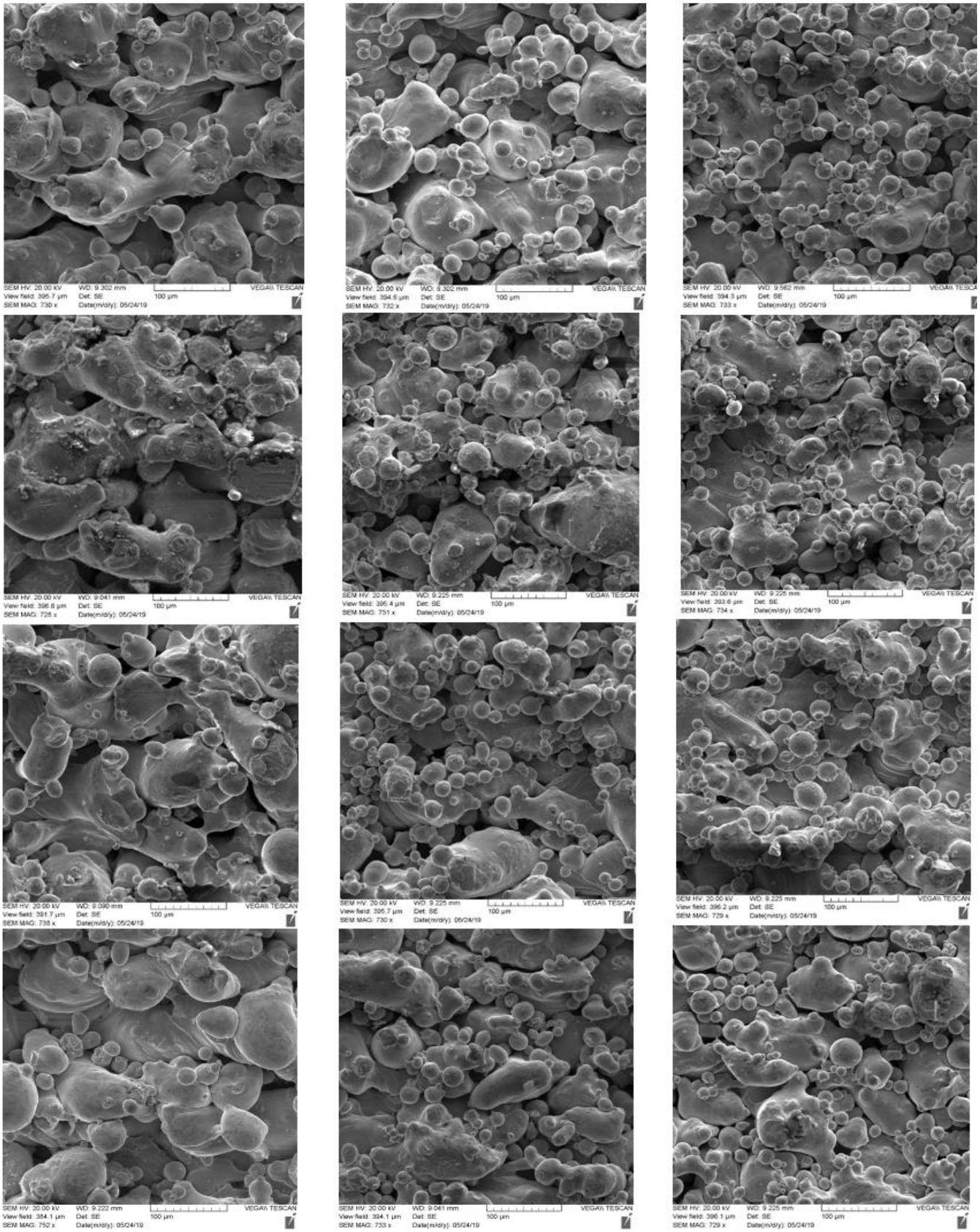

Figure 37: SEM micrographs showing microstructure of side surfaces. From left to right showing Top, Middle and Bottom layer. From Top to Bottom row showing samples D8, B5, D5 and A8 respectively

B. *Composition through EDS*

Energy-Dispersive X-Ray Spectroscopy (EDS) was used to analyze the chemical characterization of the parts without destroying the samples during the SEM analysis. Only steel substrate samples were analyzed to determine the amount of oxygen that has affected the parts. It is assumed that the parts will have a uniform oxidation spread throughout both substrates as the only external affecting factors for oxidation was the oxygen in the chamber as well as the substrate heating. As shown in Table 10, the average oxidation of the parts during printing was 6% with the lowest of part A8 is sitting at 4.43% with 39.33W/mm^3 of power. D5 with the highest power of 77.89W/mm^3 had the highest oxidation at 6.88% and can therefore be concluded that the power greatly affects the oxidation of the parts and should therefore be optimized if high purity copper is desired. Figure 38 shows the resulting peaks for the part A8 with the lowest oxygen levels which indicate high quality parts. Note that full scale for highest peak is 12804 counts.

Row Labels	Avg of C	Avg of O	Avg of Cu
A8	16.33	4.43	79.24
B5	27.95	6.88	65.17
D5	18.13	6.80	75.06
D8	17.59	5.95	76.46
Averages	**20.00**	**6.02**	**73.98**

Table 10: The Chemical composition of Cu

Using data analysis from Minitab, the hypothesis of the power negatively affecting the oxygen content is confirmed as seen in Figure 39.

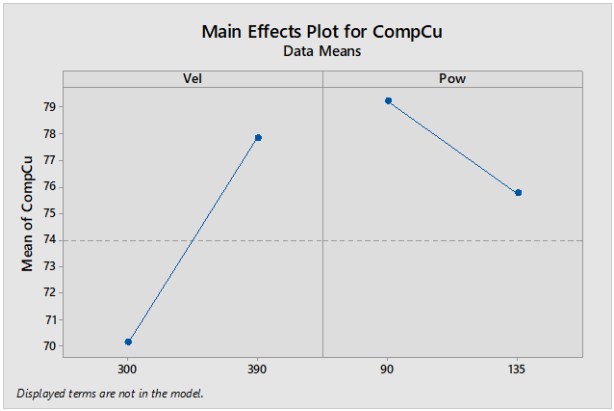

Figure 39: Effects of Power on purity of copper

C. *Redsidual Stresses through XRD*

X-Ray diffraction (XRD) was used in contrast to the prior SEM analysis, for only four of the 7 previous samples were selected. This selection also excluded their duplicates. These samples were A8, D5, B5 and D8, with estimated absorbed energy densities of ~40J/mm3, ~78J/mm3, and ~60J/mm3 respectively. It should be noted that these samples were manufactured on the steel substrate and not the copper electroplated substrate. Table 12 lists the parameters applied in the XRD analysis of the named samples. Figure 40 displays the crystallographic planes of pure copper and thereby the angles to which the samples were analyzed.

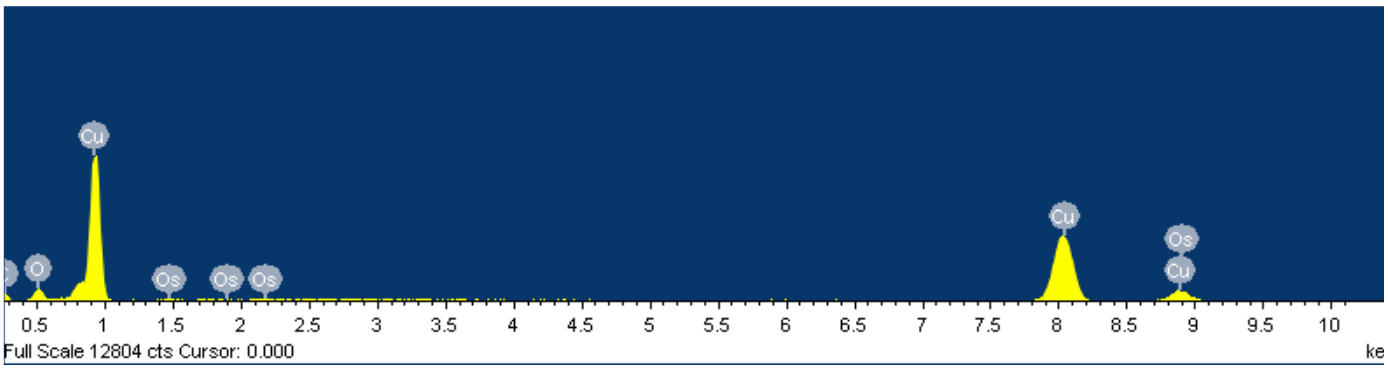

Figure 38:Spectrum of A8 with highest copper density and lowest oxygen count.

Set	Sample ID	Est. Absorbed Energy Density	Stress			Error			Principal Stress	
			X	Y	XY	X	Y	XY	Max	Min
ST2	A8	~40J/mm³	-92.7	-64.3	-14.5	7.9	7.9	5.8	-98.8	-58.2
	B5	~60J/mm³	-69	-75.9	0.6	6	5.8	4.2	-76	-68.9
	D5	~78J/mm³	-74.3	-69.6	9.4	9.8	10	7.6	-81.7	-62.2
	D8	~60J/mm³	-41.1	-43.7	8.4	7.3	6.7	5	-50.9	-33.9
ST1	A8	~40J/mm³	-122.4	-128.2	-14.8	13.2	12.4	9.6	-140.4	-110.3
	B5	~60J/mm³	-78.8	-49.6	-8.7	11.4	11.7	8	-81.2	-47.2
	D5	~78J/mm³	-65	-67.8	7.8	5.6	5.5	4	-74.4	-58.4
	D8	~60J/mm³	-69.9	-84.3	-5	8.7	7.2	6.6	-85.9	-68.3

Table 11: Results of XRD analysis of the top surface of samples A8, D5, B5, and D8

XRD Constants	Value
Miller plane [H K L]	[3 1 1]
2Theta	110.310
Poisson Ratio	0.36
Young's Modulus	115.473 GPa

Table 12: XRD Constants and their values used in the analysis of samples A8, D5, B5, and D8

The results of the analysis can be found in Table 11, as the measurements represent the biaxial stress condition it can be assumed that there is no stress in the Z direction. This assumption is valid as the X ray does not penetrate the part, only the top monolayers of the designated target. As the samples were analyzed only on their top surface as opposed to their lateral the results show as only compressive stresses and do not reflect the internal residual stresses throughout the different layers of the samples. Error in the results between both sets of samples can be attributed to diffraction errors in the technique as well as the excessive surface roughness seen in the above SEM imaging [45]. However, the compressive residual stresses observed appear to decrease in magnitude as the applied energy density increases, thereby inferring that the energy density applied did not exceed critical value. With sample ST2 D8 showing residual stresses of comparatively lower values to that of its pair B5, it appears that increased laser power results in improved residual stresses in comparison to that of increased scanning speed for the same resulting energy density. Additionally, as

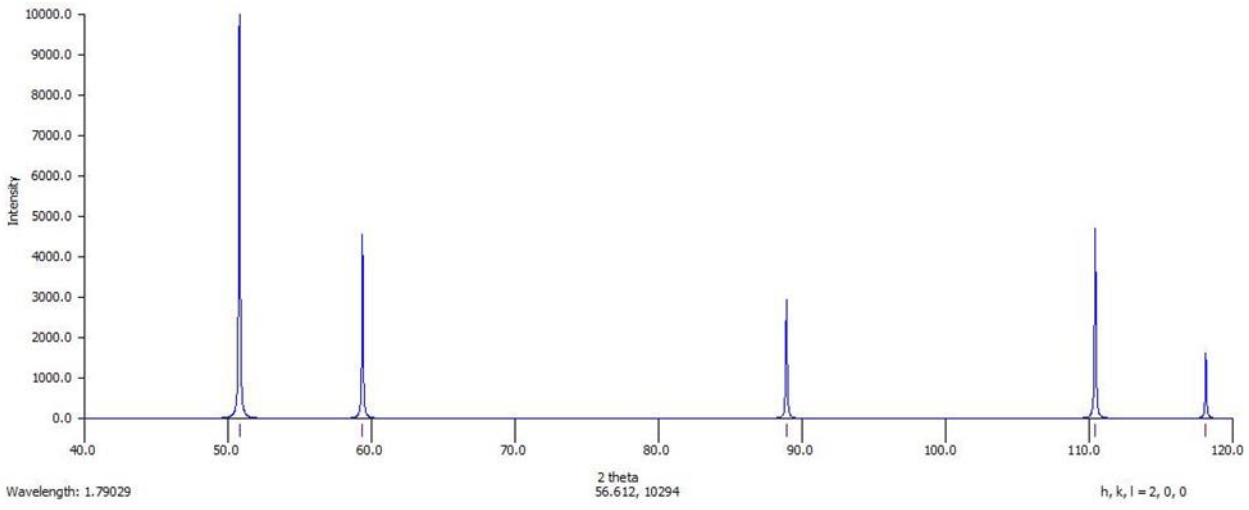

Figure 40: Crystallographic planes of pure Cu

sample D5 was set to the highest laser power and lowest scanning speed in the experiment, estimated to be just below the point of vaporization, it can be inferred that the efficiency of energy absorption was over estimated.

D. Density

As copper is primarily used for electrical applications, high density is ultimately the highest priority and therefore the aim of the manufactured part. Through this study, the SLM process has shown that high density parts are difficult to obtain and affected by the substrate too although reversed from what other authors found.

	Copper	Steel
Min	66.57%	71.17%
Avg	73.79%	74.74%
Max	76.64%	78.91%
Std.Dev	2.52%	2.02%
Var	0.06%	0.04%

Table 13: Density of parts on copper and steel substrate

Trough Table 13 it can be observed that the average density is higher for steel than with the copper plating and that minimum obtained density on steel is much higher, and outside range of error, than the comparative copper plated parts. Comparatively, power has a much larger effect on the while processing speed, velocity, has an optimized point, thereby providing simplified optimization parameters.

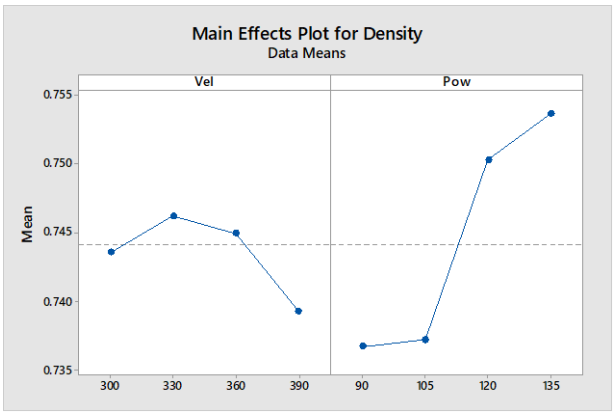

Figure 41: Effects of Power and Velocity on Density of copper

As power has the primary predictor for the density of the part, running a regression on the data provides that there should be no change to the velocity from 330mm/s and through a power increase, an increase in density should be maximized. The generated model is therefore

$$Density = 0.730 - 2.0 \times 10^{-4} Power + 3.0 \times 10^{-6} Power^2$$

Equation 7: Derived Density Equation (R^2 = 0.2930)

See Figure 43 for residuals on statistical prediction

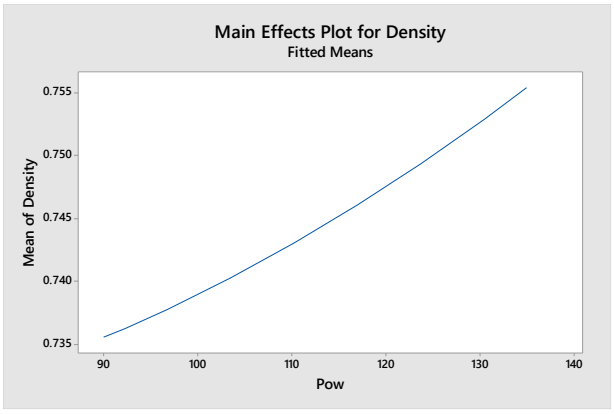

Figure 42: Predicted Density with Power

Using Figure 42, a maximum density should be reached with an increase in power before evaporation of elements occur, however this would require further study as well as the ability to remove the oxygen from the environment and part. In the Future work section the possibility of having

a high conductivity, strength and density part is highly plausible and further explained.

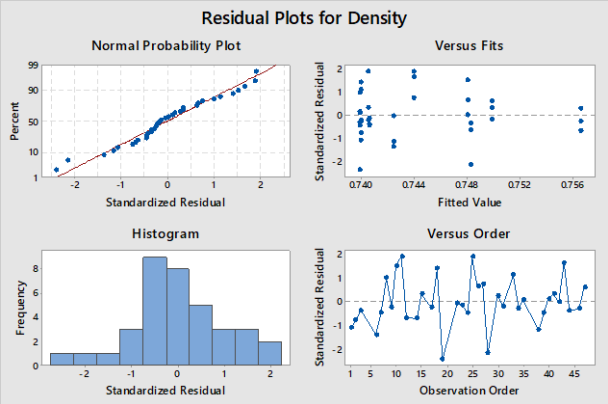

Figure 43: Residual plots for equation on Density predictions

Based off the limited data, Equation 7, has a low R^2 value though distribution is very wide and other methods with higher order predictors are far worse off. Therefore, a secondary study would be required with higher ranges in order to observe additional changes in the process and density.

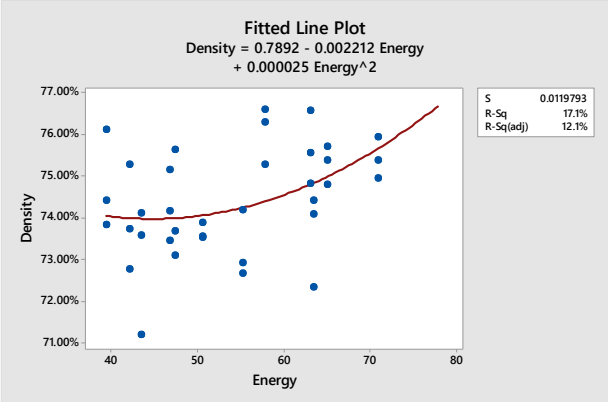

Figure 44: Sample regression with higher order for regression

Looking at the regions outlier data in the regressions run, a simplified plot as seen in Figure 45 can be used to determine optimal parameters for desired density. However, like other regressions, more data is required in order to predict density better.

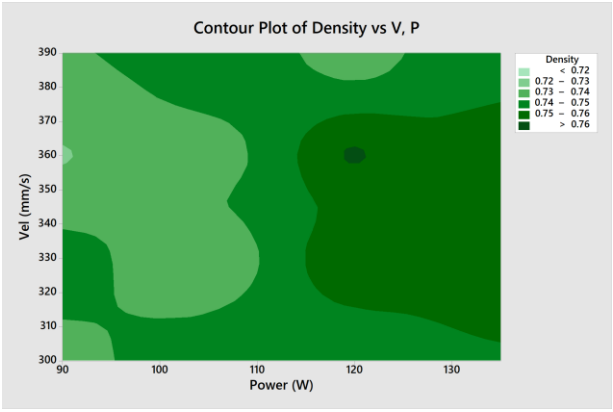

Figure 45: Simplified Plot for Power Regions

E. Combined data

XIV. FUTURE WORK

A. Material Composites for Oxidation Prevention

Roy et. al. [46] studied the particular effect of the production of the copper powder particles for the use of SLM produced nano-inks. Each of their particles were produced using different methods and therefore different morphologies as seen in Table 14.

Roy et. al. explains that the samples once created tended to agglomerate and as such tended to go as big as 120µm. This coupled with the particles oxidizing would therefore cause the defects seen in other studies as neither the powder as a base product or the final part would be of high quality due to the oxidation defects that would occur. Roy et. al. also noted that the copper particles produced by laser ablation coated with the carbon and the oxide layers tended to agglomerate while not further oxidizing. This agglomeration would still affect the printing quality as the particles are not evenly distributing and packing down once placed on a powder bed, leaving many voids in the part, thereby decreasing density once again. Roy et. al. did note however that their studies with the chemically synthesis parts with PVP had both high quality in the morphology as the particles were spherical as well as the PVP having stabilized the agglomeration would not interfere with the

production process, allowing for an even coating with excellent distribution of the nano particles. Thus, the coating of the powder and the stabilizer, i.e. PVP, agrees with El-Wardany et. al. as their speculation on porosity in the SLM process is primarily on the residual oxides in the base material. El-Wardany et. al. notes however that surface oxides are a more complicated issue as it tends to form during transportation and storage. El-Wardany et. al. suggests that to remove the surface oxides, alloying elements should be added to the feedstock that would react with the oxygen in order to eliminate the oxides.

C. *Graphene Base Materials*

Graphene has been referred to as a wonder material primarily because of its multifunctionality as a 2D-atomic crystal with unique properties. These properties include a high thermal conductivity at 5000W/m·K [47], high electron mobility at ≈40% that of copper, and a high modulus of elasticity (~ 1TPa). This in effect makes it ideal for a variety of applications. Graphene has been shown to be an excellent material for conductivity with Chyada et. al. [48] showing a 10.2% increase in conductivity when graphene was mixed with aluminium. With base carbon standard potential for CO_2 production being 0.207, compared to coppers 0.16 for CuO_2, reasonably, the expectation can be for the carbon to react with the oxygen and produce carbon dioxide, a compound not readily absorbed into copper at high temperatures. Graphene however tends to come in stacks, known as graphite and requires breakdown into graphene flakes, ribbons or sheets before becoming a useable material as the graphite is generally known as a 3D variant of graphene, present as a stable variant of soot [49].

Sample Number	Nominal Particle Size (nm)	Measured Size (nm)	Measured Sintering Temperature (°C)	Production Method	Unsintered Morphology	Coating Layer
1	40	20-400	230	Electric Explosion of Wire	Spherical, Agglomerated	None
2	100	40-300	242	Electric Explosion of Wire	Irregular, Agglomerated	None
3	25	20-340	322	Laser Ablation	Irregular, Agglomerated and Highly Fibrous	Carbon
4	25	40-670	275	Laser Ablation	Spherical, Agglomerated	Copper Oxide
5	100	20-170	330	Chemical Synthesis	Spherical	Carbon
6	90	10-210	416	Chemical Synthesis	Spherical	PVP
7	90	30-220	420	Chemical Synthesis	Spherical	PVP

Table 14: Copper Nano-Particles used for SLM production [46]

B. *Alloying Elements*

As seen in Figure 15, the alloying element greatly affects the way that the copper conducts with significant losses on as much as 1% of element added. Other elements have to be evaluated therefore to facilitate the SLM process that both allows for oxidation reduction as well as minimize the loss in the conductivity.

1. *Material Manufacting Review*

Graphene, in particular graphene flakes (GF), has been a high production graphene variant with

reliability in the production of sizes and thicknesses. Graphene flakes has been produced using varying methods with varying thicknesses and lengths, each providing a unique characteristic to the material. Kairi et. al. [50] studied multiple production processes including ball-milling, sonication, shock waves, shear in liquid and electrochemical. In their study, Kairi et. al. does not include the study of reduced graphene oxide (rGO) as GO and rGO materials produced contains many defects, thereby changing the material properties significantly. As seen in Table 15, there are several differences in the way that the graphene flakes are produced with varying success in the thickness and with little variance in the ratios of bonding, thereby signifying almost pristine materials as the I_D/I_G ratio is near that of pure graphene as the ideal I_D/I_G. ratio for graphene is 0.30 [51].

Method	Reduction Agent	Characteristics
Planetary Mill (dry)	Ammonia Borane	Single or few-layer GF (<6), I_D/I_G = 0.5
Planetary Mill (Wet)	N,N-Dimethyl-formamide	Single- and few-layer (<4), $I_D/I_G \approx$ 0.34
Explosion/ Shockwave Production	N/A – 4.4M 15% HCl purification required	Single- and few-layer. I_D/I_G = 0.06-0.12
Bath sonication	NMP	Multilayer GF (<10) I_D/I_G = 0.3-0.6
Sonification assisted electrochemical.	Perchloric acid	Few layers (3-6) I_D/I_G = 0.478

Table 15: Graphene production quality for high yield productions [50].

As Wang et. al. [52] explains, there has been several studies that uses rGO composites with copper to reinforce the copper porosity. This is due to the reaction that the rGO undergoes as rGO is approaching the pure single layer graphene structure that is desired for the best results. However, rGO is fabricated through either an oxidation then reduction process whereby the reduction happens through high temperature reactions, i.e. 1000°C or higher [53], thereby increasing the cost drastically for the rGO materials. As the SLM process creates the high temperature environment as well as provide the oxygen during the production in the melt pool as part of the $Cu2O_2$, thin layered graphene flakes (<7 layers) would suffice in both reaction and strengthening of the copper compounds. As Wang et. al. discovered, at 2.5 wt. %, the copper yield strength increased from ~250MPa to ~500MPa, as seen in Figure 46, through a sintering process.

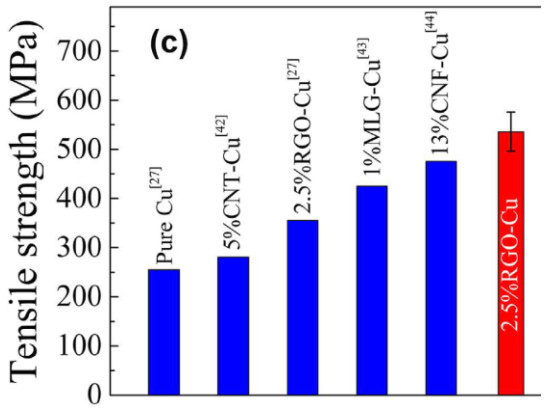

Figure 46: Tensile strength increase through the addition of rGO composites [52]

2. *Material Composistions and Expected Effects*

As copper oxides comes in varying different levels, i.e. copper(I) oxide, copper (II) oxide and copper dioxide, it is important to note that only copper (I) oxide is typically observed and present in most OFHC produced powders. With the chemical formula of Cu2O, and most OFHC powders containing less than 0.5% Cu2O, the primary oxygen source in the SLM process is the oxygen in surrounding processes. As El-Wardany et. al. explains, the ideal situation for production of copper-based parts should take place in a premixed atmosphere of 4% hydrogen and 96% argon gas to prevent any further oxidation or reoxidation of the powder. Especially since the primary oxidation happens on the outer surface of the part, and the AM process depends on the layer by layer production, its is vital to remove oxygen from each layer. Thereby, as carbon reacts on a 2:1 ratio for CO2, the limiting reactant is the available oxygen. As most systems in inert atmospheres where SLM manufacturing are done contains less than 2% oxygen by volume, the amount of graphene flakes

can be adjusted to suit the oxidation reaction as well as the desired strength of the part. For example, given an area of 250mm × 250mm x 40µm, or 2.5cm3 and the optimal density of CO being 6.0g/cm3, theoretically, the amount of oxygen available to the process would be the immediate area of the powder. Thereby using the molar weight, of 143.09g/mol, we can determine that there is 15g of Cu2O and subsequently, 1.677g of oxygen at 100% concentration. Given that, there will be a requirement of 0.625g of carbon for every full layer of exposure at 100% oxygen exposure. Calculating the adjusted value of 2% oxygen, there is only a need of 0.0125g of carbon for the full exposure of the whole layer. Thus, there is only the need for 0.8wt. % carbon in the whole layer with any extra going towards the alloying of the material. As the combustion point of graphene flakes are at 620°K [15], reasonable expectations would be that the flakes would combust due to the 1000°C and higher melt pool which would the graphene would oxidize and combust, thereby leaving the melt pool.

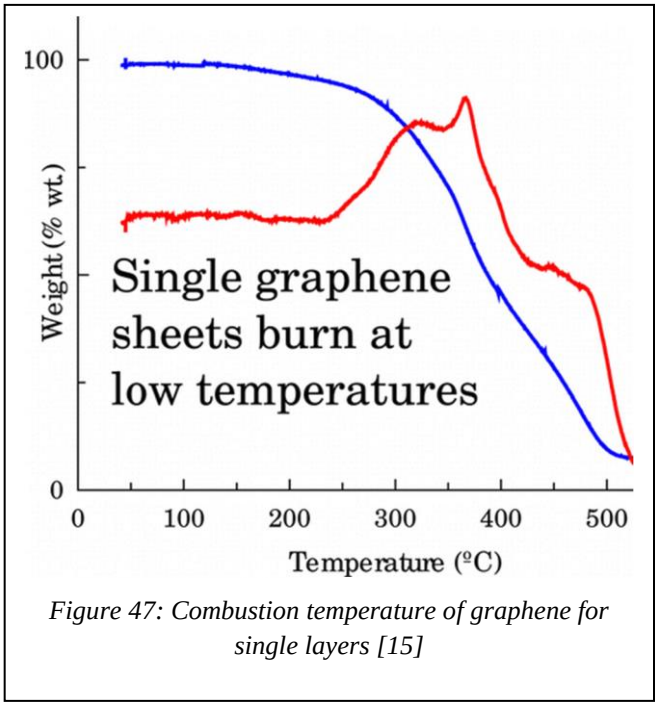

Figure 47: Combustion temperature of graphene for single layers [15]

As Koltsova [54] et. al. found, by adding between 3-5% carbon as either graphite, copper nano flakes or graphene, the hardness can significantly increase in the material. Graphene nano flakes produced an additional 20 kg/mm^2 hardness increase and Koltsova et. al. showed that the average grain size ended up at 4µm, thereby also allowing for only a 12% drop in elasticity, the best result between the tested methods as seen in Figure 48.

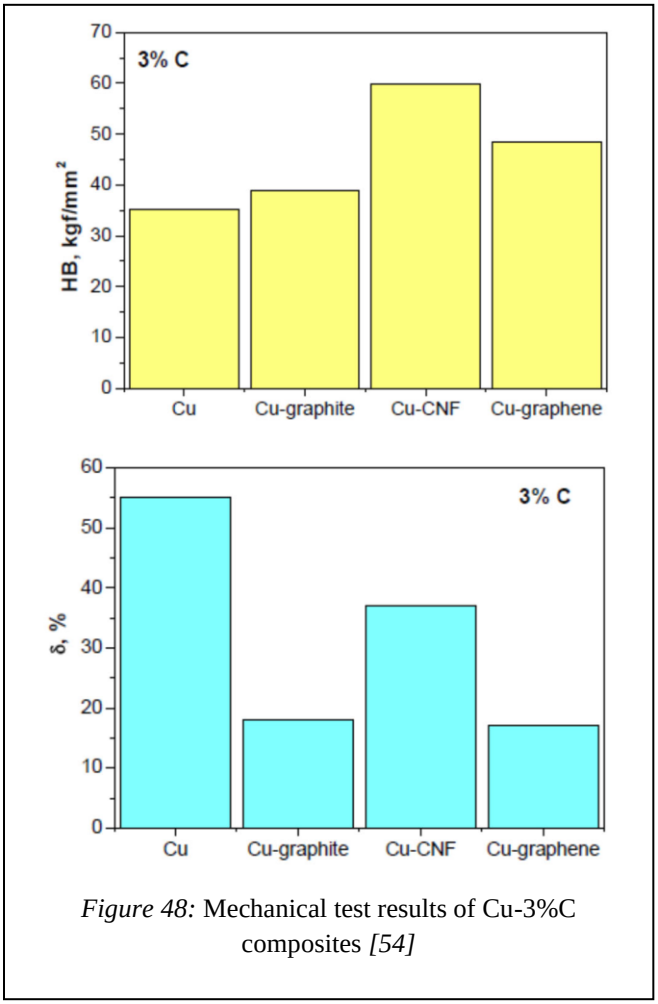

Figure 48: Mechanical test results of Cu-3%C composites *[54]*

Also, as Koltsova et. al. noted, that with the lower carbon content and smaller particle size, up to a 70% improvement could be seen in hardness and a 39% performance reduction in elasticity when limiting the layers of graphene as between 8 and 12 layers. Therefore, by limiting the layers, reducing the carbon content to lower percentages while keeping the content above the minimum required reaction content, carbon can be a big assistance in the production of copper-based materials in the AM field using the SLM process.

XV. Conclusion

XVI. REFERENCES

[1] R. F. Cochrane, E. O. Olakanmi and K. W. Dalgarno, "Densification mechanism and microstructural evolution in selective laser sintering of Al–12Si powders," *Journal of Materials Processing Technology,* vol. 211, no. 1, pp. 113-121, 2011.

[2] N. Read, Wang W, K. Essa and M. Atallah, "Selective laser melting of AlSi10Mg alloy: Process optimisation and mechanical properties development," *Materials & Design (1980-2015),* vol. 65, pp. 417-424, 2015.

[3] M. Ma, Z. Wang, M. Gao and X. Zeng, "Layer thickness dependence of performance in high-power selective laser melting of 1Cr18Ni0Ti stainless steel," *Journal of Materials Processing Technology,* vol. 215, pp. 142-150, 2015.

[4] L. N. Carter, X. Wang, N. Read, R. Khan, M. Aristizabal, K. Essa and M. M. Attallah, "Process optimization of selective laser melting using energy density model for nickel based superalloys," *MATERIALS SCIENCE AND TECHNOLOGY,* vol. 32, no. 7, pp. 657-661, 2016.

[5] K. Dalgarno and C. S. Wright, "Approaches to processing metals and ceramics through the laser scanning of powder beds-a review," *Powder Metallurgy Processess,* vol. 1, pp. 70-79, 2001.

[6] P. Fischer, M. Locher, V. Romano, H. P. Weber, S. Kolossov and R. Glardon, "Temperature measurements during selective laser sintering of titanium powder," *International Journal of Machine Tools & Manufacture,* vol. 44, pp. 1293-1296, 2004.

[7] TWI, "WELDING OF COPPER AND ITS ALLOYS - PART 1 - Job Knowledge 111 - TWI," TWI Ltd , 2019. [Online]. Available: https://www.twi-global.com/technical-knowledge/job-knowledge/welding-of-copper-and-its-alloys-part-1-111. [Accessed 4 4 2019].

[8] X. Cao, W. Wallace, J. P. Immarigeon and C. Poon, "Research and Progress in Laser Welding of Wrought Aluminum Alloys. II. Metallurgical Microstructures, Defects, and Mechanical Properties," *Materials and Manufacturing Processes* , vol. 18, no. 1, pp. 23-49, 2003.

[9] The Engineering Toolbox, "Solids - Volume Temperature Expansion Coefficients," [Online]. Available: https://www.engineeringtoolbox.com/volum-expansion-coefficients-solids-d_1894.html. [Accessed 4 4 2019].

[10] J. Campbell, "Review of fluidity concepts in casting," *Cast Metals,* vol. 7, no. 4, pp. 227-237, 1995.

[11] J. Campbell, Castings, Elsevier, 2003.

[12] E. Louvis, P. Fox and C. J. Sutchliffe, "Selective laser melting of aluminium components," *Journal of Materials Processing Technology,* vol. 211, pp. 275-284, 2011.

[13] M. I. Redondo and C. B. Breslin, "Polypyrrole Electrodeposited on Copper from an Aqueous Phosphate Solution," *Corrosion Science,* vol. 49, pp. 1765-1776, 2007.

[14] S. Chen, L. Brown, M. Levendorf, W. Cai, S.-Y. Ju, J. Edgeworth, X. Li, C. W. Magnuson, A. Velamakanni, R. D. Piner, J. Kang, J. Park and R. S. Ruoff, "Oxidation Resistance of Graphene-Coated Cu and Cu/Ni Alloy," *American Chemical Society,* vol. 5, no. 2, pp. 1321-1327, 2011.

[15] A. Eftekhari and P. Jafarkhani, "urly Graphene with Specious Interlayers Displaying Superior Capacity for Hydrogen Storage," *Journal of Physical Chemistry* , vol. 117, no. 48, pp. 25845-25851, 2013.

[16] M. M. Collur, A. Paul and T. Debroy, "Mechanism of alloying element vaporization during laser welding," *Metallurgical Transactions B,* vol. 18, no. 4, pp. 733-740, 1987.

[17] D. Buchbinder, H. Schleifenbaum, S. Heidrich, W. Meiners and J. Bültmann, "High Power Selective Laser Melting (HP SLM) of Aluminum Parts," *Physics Procedia,* vol. 12, pp. 271-278, 2011.

[18] P. Mercelis and J. Kruth, "Residual stresses in selective laser sintering and selective laser melting," *Rapid Prototyping Journal,* vol. 12, no. 5, pp. 254-265, 2006.

[19] D. Gu, Y.-C. Hagedorn, W. Meiners, G. Meng, R. J. Santos Batista, K. Wissenbach and R. Poprawe, "Densification behavior, microstructure evolution, and wear performance of selective laser melting processed commercially pure titanium," *Acta Materialia,* vol. 60, no. 9, pp. 3489-3860, 2012.

[20] M. Agarwala, D. Bourell, J. Beaman, H. Marcus and J. Barlow, "Direct selective laser sintering of metals," *RAPID PROTOTYPING JOURNAL,* vol. 1, no. 1, pp. 26-36, 1995.

[21] J. P. Kruth, L. Froyen, J. van Vaerenbergh, P. Mercelis, M. Rombouts and B. Lauwers, "Selective laser melting of iron-based powder," *Journal of Materials Processing Technology,* vol. 149, no. 1-3, pp. 616-622, 2004.

[22] E. Chlebus, B. Kuźnicka, T. Kurzynowski and B. Dybała, "Microstructure and mechanical behaviour of Ti—6Al—7Nb alloy produced by selective laser melting," *Materials Characterization,* vol. 65, no. 5, pp. 488-495, 2011.

[23] A. B. Spierings, N. Herres and G. Levy, "Influence of the particle size distribution on surface quality and mechanical properties in AM steel parts," *Rapid Prototyping Journal,* vol. 17, no. 3, pp. 195-202, 2011.

[24] Y. Wang, J. Bergström and C. Burman, "Characterization of an iron-based laser sintered material," *Journal of Materials Processing Technology,* vol. 172, no. 1, pp. 77-87, 2006.

[25] D. Q. Zhang, Z. H. Liu and C. K. Chua, "Investigation on forming process of copper alloys via Selective Laser Melting," in *High Value Manufactuing,* 2012, pp. 1-15.

[26] Technology Strategy Board, High Value Manufacturing, CRC Press, 2012, pp. 1-15.

[27] F. Sciammarella, M. J. Gonser and M. Styrcula, "Laser Additive Manufacturing of Pure Copper," 2012.

[28] T. El-Wardany, Y. She, V. Jagdale, J. K. Garofano, J. Liou and W. Schmidt, "CHALLENGES IN 3D PRINTING OF HIGH CONDUCTIVITY COPPER," in *Proceedings*

of the ASME 2017 International Technical Conference and Exhibition on Packaging and Integration of Electronic and Photonic Microsystems, San Francisco, California, 2017.

[29] D. Gu and Y. Shen, "Balling phenomena during direct laser sintering of multi-component Cu-based metal Powders," *Alloys Comp.,* vol. 432, no. 1,2, pp. 163-166, 2007.

[30] Georgia State University, "Thermal Conductivity," [Online]. Available: http://230nsc1.phy-astr.gsu.edu/hbase/Tables/thrcn.html. [Accessed 8 4 2019].

[31] Georgia State University, "Standard Electrode Potentials," [Online]. Available: http://230nsc1.phy-astr.gsu.edu/hbase/Tables/electpot.html. [Accessed 8 4 2019].

[32] P. Frigola, O. A. Harrysson, T. J. Horn, H. A. West, R. L. Aman, J. M. Rigsbee, D. A. Ramirez, L. E. Murr, F. Medina, R. B. Wicker and E. Rodriguez, "Fabricating Copper Components with Electron Beam Melting," in *Proceedings of EPAC08*, Genoa, Italy,, 2008.

[33] P. Anne Marie Helmenstine, "Table of Electrical Resistivity and Conductivity," ThoughtCo.com, 24 09 2018. [Online]. Available: https://www.thoughtco.com/table-of-electrical-resistivity-conductivity-608499. [Accessed 06 04 2019].

[34] D. Chapman, High Conductivity Copper for Electrical Engineering, Hemel Hempstead: Copper Development Association, 2016.

[35] M. F. Ashby, Materials and the Environment -, Butterworth-Heinemann, 2013.

[36] C. T. Kwok, "Pulsed laser surface treatment of multilayer gold–nickel–copper (Au/Ni/Cu) coatings to improve the corrosion resistance of components in electronics," in *Laser Surface Modification of Alloys for Corrosion and Erosion Resistance*, Woodhead Publishing, 2012, pp. 109-123.

[37] M. Yakout, A. Cadamuro, M.A.Elbestawi and S. C.Veldhuis, "The selection of process parameters in additive manufacturing for aerospace alloys," *Journal of Materials Processing Technology*, vol. 92, no. 5-8, pp. 2081-2098, 2017.

[38] M. Yakout, M. Elbestawi and S. C. Veldhuis, "A study of thermal expansion coefficients and microstructure during selective laser melting of Invar 36 and stainless steel 316L," *Additive Manufacturing*, vol. 24, pp. 405-418, 2018.

[39] T. DebRoy, H. Wei, J. Zuback, T. Mukherjee, J. Elmer, J. Milewski, A. Beese, A. Wilson-Heid, A. De and W. Zhang, "Additive manufacturing of metallic components – Process Structure and Properties," *Progress in Materials Science*, vol. 92, pp. 112-224, 2018.

[40] P. A. Lykov, E. V. Safonov and A. M. Akhmedianov, "Selective Laser Melting of Copper," *Materials Science Forum*, vol. 843, pp. 284-288, 2015.

[41] F. Sciammarella, M. J. Gonser and M. Styrcula, "Laser Additive Manufacturing of Pure Copper," *RAPID*, pp. 143-162, 2013.

[42] M. A. Lodes, R. Guschlbauer and C. Körner, "Process development for the manufacturing of 99.94% pure copper via selective electron beam melting," *Materials Letters*, vol. 143, pp. 289-301, 2015.

[43] T. Scharowsky, V. Juechter, R. F. Singer and C. Körner, "Influence of the Scanning Strategy on the Microstructure and Mechanical Properties in Selective Electron Beam Melting of Ti–6Al–4V," *Advanced Engineering Materials,* vol. 17, no. 11, 2015.

[44] "Conductivity Materials," Copper Development Association, [Online]. Available: https://copperalliance.org.uk/about-copper/conductivity-materials/. [Accessed 06 04 2019].

[45] P. S. Prevéy, "X-ray Diffraction Residual Stress Techniques," *Metals Park: American Society for Metals,* vol. Metals Handbook, no. 10, pp. 380-392, 1986,.

[46] N. K. Roy, C. S. Foong and M. A. Cullinan, "Effect of size, morphology, and synthesis method on the thermal and sintering properties of copper nanoparticles for use in microscale additive manufacturing processes," *Additive Manufacturing,* vol. 21, pp. 17-29, 2018.

[47] A. A. Balandin, S. Ghosh, W. Bao, I. Calizo, D. Teweldebrhan, F. Niao and C. N. Lau, "Superior Thermal Conductivity of Single-Layer Graphene," *Nano Letterrs,* vol. 8, no. 3, pp. 902-907, 2008.

[48] F. A. Chyada, A. R. Jabur and H. A. Alwan, "Effect addition of graphene on electrical conductivity and tensile strenght of recycled electric power transmission wires," in *International Conference on Technologies and Materials for Renewable Energy, Environment and Sustainability*, Beirut Lebanon, 2017.

[49] A. Geim and A. MacDonald , "Graphene: Exploring carbon flatland," *Physics Today,* vol. 6, no. 8, p. 35, 2007.

[50] M. I. Kairi, S. Dayou, N. I. Kairi, S. A. Bakar, B. Vigolo and A. R. Mohamed, "Toward high production of graphene flakes – a review on recent developments in their synthesis methods and scalability," *Journal of Materials Chemistry A,* vol. 6, pp. 15010-15026, 2018.

[51] Instanano, "Raman Spectroscopy Characterization of Graphene & Graphene Oxide," [Online]. Available: http://instanano.com/characterization/experimental/raman-graphene/. [Accessed 8 4 2019].

[52] L. Wang, Z. Yang, Y. Cui, B. Wei, C. Xu, J. Sheng, M. Wang, Y. Zhu and W. Fei, "Graphene-copper composite with micro-layered grains and ultrahigh strength," *Scientific Reports,* vol. 7, p. Art 41896 , 2017.

[53] J. de La Fuente, "Reduced Graphene Oxide - What Is It? How Is It Created?," Graphenea, [Online]. Available: https://www.graphenea.com/pages/reduced-graphene-oxide. [Accessed 8 4 2019].

[54] T. S. Koltsova, L. I. Nasibulina, I. V. Anoshkin, V. V. Mushin, E. I. Kauppinen, O. V. Tolochko and A. G. Nasibulin, "New Hybrid Copper Composite Materials Based on Carbon Nanostructures," *Journal of Materials Science and Engineering B,* vol. 4, pp. 240-246, 2012.

[55] E. Brandl, U. Heckenberger, V. Holzinger and D. Buchbinder, "Additive manufactured AlSi10Mg samples using Selective Laser Melting (SLM): Microstructure, high cycle fatigue, and fracture behavior," *Materials & Design,* vol. 34, pp. 159-169, 2012.

[56] R. Konečnáa, G. Nicolettob, L. Kunzc and A. Bača, "Microstructure and directional fatigue behavior of Inconel 718 produced by selective laser melting," *Procedia Structural Integrity* , vol. 2, p. 2381–2388, 2016.